

VILNIUS UNIVERSITY

Darius Baronas

COMPUTER AIDED MODELLING OF MULTILAYER BIOSENSORS AND
OPTIMIZATION BASED PROCESSING OF AMPEROMETRIC
MEASUREMENTS

Doctoral Dissertation
Physical Sciences, Informatics (09 P)

Vilnius, 2014

Doctoral dissertation was prepared in 2009 - 2013 at the Institute of Mathematics and Informatics of Vilnius University.

Scientific Supervisor:

Prof. Dr. Habil. Antanas Žilinskas (Vilnius University, Physical Sciences, Informatics - 09 P).

Scientific Consultant:

Prof. Dr. Habil. Feliksas Ivanauskas (Vilnius University, Physical Sciences, Informatics - 09 P).

VILNIAUS UNIVERSITETAS

Darius Baronas

DAUGIASLUOKSNIŲ BIOJUTIKLIŲ KOMPIUTERINIS MODELIAVIMAS IR
OPTIMIZAVIMO METODAIS GRĮSTA MATAVIMŲ METODIKA

Daktaro disertacija
Fiziniai mokslai, informatika (09 P)

Vilnius, 2014

Disertacija rengta 2009 - 2013 metais Vilniaus universiteto Matematikos ir informatikos institute.

Mokslinis vadovas:

prof. habil. dr. Antanas Žilinskas (Vilniaus universitetas, fiziniai mokslai, informatika - 09 P).

Mokslinis konsultantas:

prof. habil. dr. Feliksas Ivanauskas (Vilniaus universitetas, fiziniai mokslai, informatika - 09 P).

Acknowledgements

I would like to thank my doctoral dissertation scientific supervisor Prof. Dr. Habil. Antanas Žilinskas and scientific consultant Prof. Dr. Habil. Feliksas Ivanauskas for their effort and input.

Table of Contents

| | |
|--|-----------|
| Introduction | 9 |
| Aim | 10 |
| Methodology | 10 |
| Scientific novelty and results | 11 |
| Practical value | 11 |
| Proposition statements to defend | 12 |
| Publications by the Author | 13 |
| Thesis structure | 15 |
| 1 Theoretical base of a biosensor | 16 |
| 1.1 Biosensors | 16 |
| 1.2 Mathematical modelling of biosensors | 17 |
| 1.2.1 Governing equations | 18 |
| 1.2.2 Initial conditions | 19 |
| 1.2.3 Dimensionless model | 20 |
| 1.3 Numerical biosensor solution | 21 |
| 1.3.1 Biosensor current | 22 |
| 1.3.2 Reaction time of the model | 22 |
| 1.3.3 Flow injection analysis | 23 |
| 1.3.4 Biosensor sensitivity | 24 |
| 1.4 Chapter summary | 26 |
| 2 Biosensor modelling | 28 |
| 2.1 Amperometric biosensors in flow injection analysis systems | 28 |
| 2.1.1 Mathematical model | 29 |
| 2.1.2 Governing equations | 29 |
| 2.1.3 Initial and boundary conditions | 30 |
| 2.1.4 Biosensor response | 31 |
| 2.1.5 Dimensionless model | 32 |
| 2.1.6 Numerical simulation | 35 |
| 2.1.7 Results and discussion | 37 |
| 2.1.8 Section summary | 41 |
| 2.2 Modelling and simulation of amperometric biosensors acting in the flow injection analysis | 42 |
| 2.2.1 Biosensor structure | 43 |

| | | |
|----------|--|-----------|
| 2.2.2 | Mathematical model | 44 |
| 2.2.3 | Governing equations | 44 |
| 2.2.4 | Initial conditions | 46 |
| 2.2.5 | Boundary conditions | 46 |
| 2.2.6 | Biosensor response | 47 |
| 2.2.7 | Characteristics of Biosensor Response | 48 |
| 2.2.8 | Dimensionless Model | 49 |
| 2.2.9 | Numerical simulation | 52 |
| 2.2.10 | Results and discussion | 55 |
| 2.2.11 | Section summary | 58 |
| 2.3 | Computational modelling and validation of a multilayer amperometric biosensor | 59 |
| 2.3.1 | Mathematical model | 60 |
| 2.3.2 | Governing equations | 61 |
| 2.3.3 | Initial and boundary conditions | 63 |
| 2.3.4 | Biosensor response | 65 |
| 2.3.5 | Dimensionless model | 66 |
| 2.3.6 | Numerical simulation | 68 |
| 2.3.7 | Results and discussion | 69 |
| 2.3.8 | Section summary | 72 |
| 3 | Quantitative analysis of mixtures | 74 |
| 3.1 | Optimization-Based Evaluation of Concentrations in modelling the Biosensor-Aided Measurement | 74 |
| 3.1.1 | Mathematical model | 75 |
| 3.1.2 | Biosensor response | 77 |
| 3.1.3 | Generated data | 77 |
| 3.1.4 | Analysis of the available data | 79 |
| 3.2 | Analysis of the properties of the mathematical model | 81 |
| 3.3 | Statement of the relevant optimization problem | 85 |
| 3.4 | Numerical experiments | 88 |
| 3.5 | Further development of the biosensor model | 90 |
| 3.5.1 | Mathematical model | 90 |
| 3.5.2 | Governing equations | 92 |
| 3.5.3 | Initial and boundary conditions | 92 |
| 3.5.4 | Biosensor response | 93 |
| 3.6 | Section summary | 94 |
| | Conclusions | 95 |
| | List of references | 97 |

Introduction

A biosensor is an analytical device that inverts a biochemical reaction process into a measurable signal using transducer [1–3]. Biosensors can be used for detecting various substances like pollutants, metabolites, microbial load, etc. Usually a biosensor consists of two elements: a biological sensing element and a transducer for detecting the analyte concentration.

The first biosensor was introduced in 1956 by Professor Leland C. Clark Jr. and he is known as the founder of the biosensor concept. For the first time biosensors became commercial in 1975. A glucose analyser based on the amperometric detection of hydrogen peroxide, was launched. During the past 40 years, various biosensors have been researched and developed involving a wide range of applications, although the number of commercially available biosensors is limited. Biosensor technology is developing, so we can expect that biosensors will become more widely available commercially. The market size of biosensors is growing: according to Global Biosensors Market in 2007 it was 10 billion US\$ and by the year 2015 it is forecasted to reach 12 billion US\$, mainly because of the growing population and an increasing number of people affected with various diseases [4].

These devices are wide used in industry for process monitoring and control, particularly, food and drink, in the military cases for battlefield monitoring of poison gases, nerve agents, and people [5–7]. It is common to use them in medicine because they are highly sensitive, their biological recognition is usually very selective, inexpensive, stable and reliable, providing an opportunity to instantly identify relevant biocomponents, i.e. hormones, drugs, etc. [8, 9] Commonly they are used in medicine to measure the sugar quantity in blood [10, 11], and to make a genetic analysis in hospitals [12].

Biosensors have a lot of advantages compared to usual biological methods of

analysis - biosensors are small, simple to use, radioactivity proof, etc. These characteristics make them attractive to use [13].

When solving a biosensor model, usually nonlinear diffusion equations are used that are not analytically solved. Numerical methods are also used, usually finite difference methods. To investigate biosensors, computer-aided models are created [14].

Aim and object of the study

The aim of the research was to develop numerical models of layered amperometric biosensors, develop software tool for computational modelling as well as develop an algorithm for the quantitative analysis of biosensor responses to mixtures of compounds. In solving the task, the following subtasks were identified:

- Develop mathematical and numerical models of practical amperometric biosensors with multiple diffusion layers.
- Create a computer tool for the developed numerical models.
- Investigate peculiarities of responses of modelled biosensors and to identify conditions that improve the biosensor properties.
- Develop an algorithm for evaluating concentrations from the biosensor responses to mixtures of compounds.

Methodology

The biosensing systems are modelled by non-stationary reaction-diffusion equations containing nonlinear terms related to the kinetics of enzymatic reac-

tions [15, 16]. Different schemes of a biosensor were selected, with different physical parameters. To achieve goals, a number of computer experiments were carried out. Computer models were developed in the ANSI C language [17, 18]. Computations were performed using supercomputer.

Scientific novelty and results

- The existing mathematical model of an amperometric biosensor, acting in the injection mode, has been generalized to take into consideration the external mass transport by diffusion in a dialysis membrane as well as in buffer solution.
- A computational model of an amperometric mediated biosensor based on an enzyme layer and two supporting porous membranes, has been developed and validated by experimental data.
- The half maximum effective concentration, signifying the efficiency of the analysed biosensors, has been determined for different model parameters of the analysed biosensors.
- The task to evaluate concentrations of compounds, using the biosensor responses to mixtures of compounds, has been formulated and solved by using optimization based processing of amperometric measurements.

Practical value

A number of mathematical and computer models have been developed that provide an opportunity to study characteristics of amperometric biosensors to define parameters of the selected biosensors, to optimize the structure of

the biosensor without performing many expensive biochemical reactions in a laboratory. The solutions were found considering dimensionless models, and generalized results of the research are presented. The results, presented in this thesis, were used to achieve the goals of the following projects:

- “Development of bioelectrocatalysis for synthesis and analysis (BIOSA)”, funded by a grant (No. PBT-04/2010) from the Research Council of Lithuania (2008-2010).
- “Theoretical and engineering aspects of e-service technology development and application in high-performance computing platforms” (No. VP1-3.1-ŠMM-08-K-01-010) funded by the European Social Fund.
- “Support for scientists and Researchers (Global Grant measure)” (No. VP1-3.1-ŠMM-07-K) funded by the European Social Fund.

Statements to be defended

- The dimensionless mathematical modelling can be used as a framework for numerical investigation of the impact of model parameters on the biosensor action.
- The computational model of the amperometric mediated biosensor, based on an enzyme layer and two supporting porous membranes, can be successfully applied to investigate kinetic peculiarities of the biosensor.
- By increasing the thickness of the external diffusion layer or by decreasing the substrate diffusivity in this layer, the calibration curve of the biosensor can be prolonged by a few orders of magnitude.

- The calibration curve of the biosensor, acting in the injection mode, can be prolonged by a few orders of magnitude only by decreasing the injection time.
- Optimisation based analysis can be applied to the quantitative analysis of mixtures.

Publications of the Author

Periodicals

The results were published in periodic journals with a citation index of the Institute for Scientific Information. The contribution of the author is the development of numerical models, software prepared for the modelling task, solving models, getting and validating as well as analysis of the results, defining the results in written form where a various scope of the text was prepared for publication by the thesis author.

1. Baronas, Darius; Ivanauskas, Feliksas; Baronas, Romas. Mechanisms Controlling the Sensitivity of Amperometric Biosensors in Flow Injection Analysis Systems, *Journal of Mathematical Chemistry*. Dordrecht : Springer Netherlands. ISSN 0259-9791. 2011, vol. 49, no. 8, p. 1521-1534. [ISI]
2. Žilinskas, Antanas; Baronas, Darius. Optimization-Based Evaluation of Concentrations in Modelling the Biosensor-Aided Measurement, *Informatika*, Vilnius University Institute of Mathematics and Informatics. Vilnius. ISSN 0868-4952. 2011, vol. 22, no. 4, p. 589-600. [ISI]
3. Baronas, Romas; Kulys, Juozas; Žilinskas, Antanas; Lancinskas, Algirdas; Baronas, Darius. Optimization of The Multianalyte Determination With

Biased Biosensor Response, Chemometrics and Intelligent Laboratory Systems. Amsterdam : Elsevier BV. ISSN 0169-7439. 2013, vol. 126, p. 108-116. [ISI]

Peer reviewed conference publications

The presentations were presented at two international conferences:

1. Baronas, Darius; Žilinskas, Antanas; Ivanauskas, Feliksas. Computational modelling and validation of a multilayer amperometric biosensor, XVIII international master and phd student's conference "Information Society and University Studies" (IVUS 2013), April 25, 2013, Kaunas, Lithuania.
2. Baronas, Romas; Baronas, Darius. Modelling and simulation of amperometric biosensors acting in the flow injection analysis. European Modelling and Simulation Symposium, September 25-27, 2013, Athens, Greece

In addition, the results were published in the proceedings of the conferences:

1. Baronas, Darius; Žilinskas, Antanas; Ivanauskas, Feliksas. Computational modelling and validation of a multilayer amperometric biosensor. Proceedings of the XVIII international master and phd students conference "Information Society and University Studies" (IVUS 2013): Kaunas, Lithuania, 25 April 2013. Printed: 2013, p. 22-26. ISSN 2029-4824
2. Baronas, Romas; Baronas, Darius. Modelling and simulation of amperometric biosensors acting in the flow injection analysis. Proceedings of the European Modelling and Simulation Symposium, September 25-27, 2013, Athens, Greece. Eds.: A.G. Bruzzone, E. Jimenez, F. Longo, Y. Merkurjev. Printed: Render (CS), Italy, September 2013, p. 107-114. ISBN 978-88-97999-16-4

Thesis structure

The dissertation consists of the following parts: three chapters, conclusions, and the list of references.

The first chapter is a short introduction of the amperometric biosensor. The dimensions of the biosensor used in the dissertation are discussed.

In the second chapter, the results of the biosensor characteristics are discussed. In this chapter, the selected biosensors are discussed and mathematical models are introduced as well. In the first section, a model with a diffusion layer is discussed. In the enzyme layer we consider the enzyme-catalyzed reaction. In the second section, a further development of the model is introduced. In the third section, a model of a multilayer biosensor is studied. In the enzyme layer, we consider a two-stage enzyme-catalyzed reaction where the substrate combines with an enzyme to form a product in the presence of a mediator. On the electrode surface the mediator is electrochemically re-oxidised and electrons are released creating the current as an output result.

The third chapter discusses a mixture of substrates (components), each performing a biochemical reaction where the mixture of substrates combines reversibly with an enzyme to yield a product.

Chapter 1

Theoretical base of a biosensor

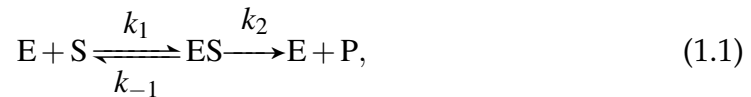
1.1 Biosensors

The biosensor is a device which is capable to transform a biochemical reaction result to analytically readable information. Analysis information depends on the amount of product formed during the biochemical reaction. Usually it consists of two components: a biochemical recognition system (bioreceptor) and a physicochemical transducer. In biosensors the recognition system utilizes a biochemical mechanism [19, 20]. The bioreceptor converts the biochemical result, which is usually an analyte concentration, into a physical signal with a defined sensitivity. The transducer is a part of the biosensor which converts receptor output in to an electric signal. Biosensors are classified by a bioreceptor and transducer. In a biosenor such as a bioreceptor, an enzyme, antibody, nucleic acid, lectins, hormone, the cell structure or tissue can be used. Enzymes are often used in developing biosensors. Dependent on a transducer, systems can be grouped in to electrochemical, optical, piezoelectric, thermometric, ion-sensitive, magnetic or acoustic ones [20, 21]. An electrochemical biosensor, when biochemical reactions between an immobilized biomolecule and target analyte produce

or consume ions or electrons, which affects the measurable electric current [22]. Electrochemical biosensors are divided into amperometric and potentiometric ones. Amperometric biosensors are most widely used, they are very sensitive and more suitable for mass production than the potentiometric ones [23–27]. The amperometric biosensor is an electronic signal converter with biochemically active substance usually enzyme. The operation of the amperometric biosensors is based on calculating the Faraday current, which is calculated while the current at the electrode is set constant. The current arises because of the oxidation or reduction of the product [28–30]. Generally the process is modelled using Michael-Menten kinetic equations.

1.2 Mathematical modelling of biosensors

The amperometric biosensor is considered as an electrode and a relatively thin layer of an enzyme (enzyme membrane) applied to the electrode surface [31]. The biosensor model involves three regions: the enzyme layer (membrane), where the enzymatic reaction as well as the mass transport by diffusion takes place, a diffusion limiting region, where only the diffusion takes place, and a convective region. In the enzyme layer we consider the enzyme-catalyzed reaction



where k_1 , k_{-1} , k_2 are the speed constants of the reaction. The substrate (S) combines reversibly with an enzyme (E) to form a complex (ES). The complex then dissociates into the product (P) and the enzyme is regenerated [32, 33].

In view of the quasi steady-state approximation, the concentration of the intermediate complex (ES) does not change and may be neglected when modelling

the biochemical behaviour of biosensors [19, 33, 34]. In the resulting scheme, the substrate (S) is enzymatically converted to the product (P),



1.2.1 Governing equations

Due to the symmetrical geometry of the electrode and a homogeneous distribution of the immobilized enzyme in the enzyme layer of a uniform thickness, a mathematical model of the biosensor action can be defined in a one-dimensional-in-space domain [15, 16, 35]. Coupling the enzyme catalyzed reaction (1.2) in the enzyme layer with the mass transport by diffusion, described by Fick's law, leads to the following system of equations:

$$\frac{\partial S}{\partial t} = D_S \frac{\partial^2 S}{\partial x^2} - \frac{V_{\max} S}{K_M + S}, \quad (1.3a)$$

$$\frac{\partial P}{\partial t} = D_P \frac{\partial^2 P}{\partial x^2} + \frac{V_{\max} S}{K_M + S}, \quad x \in (0, d), \quad t > 0, \quad (1.3b)$$

where x and t stand for a space and time, $S(x, t)$ and $P(x, t)$ are the concentrations of the substrate (S) and the product (P) in the enzyme layer, D_S , D_P are the diffusion coefficients, V_{\max} is the maximal enzymatic rate attainable with that amount of the enzyme, when the enzyme is fully saturated with the substrate, K_M is the Michaelis constant, and d is the thickness of the enzyme layer [15, 36, 37]. The Michaelis constant K_M is the concentration of the substrate at which the reaction rate is half of its maximum value V_{\max} .

1.2.2 Initial conditions

Initial conditions define the biosensor model conditions in the bulk solution [38–40]. The site where $x = 0$ is considered as the surface of electrode and $x = d$ is the boundary of the biosensor model, where the analyzed solution and enzyme membrane intercept. The activity is followed when the amount of the substrate appears on the surface of the enzyme membrane. This state of the biosensor is expressed by the initial condition parameters ($t = 0$):

$$S(x, 0) = 0, \quad P(x, 0) = 0, \quad x \in [0, d), \quad (1.4a)$$

$$S(x, d) = S_0, \quad P(x, d) = P_0, \quad x \in [0, d), \quad (1.4b)$$

where S_0 and P_0 are the substrate concentration in the bulk solution.

Due to the electrode polarization, the concentration of the product, as $x = 0$, is being constantly reduced to zero,

$$P(0, t) = 0, \quad t > 0, \quad (1.5)$$

At the electrode surface the reaction is not observed. The boundary condition for the substrate is defined as follows:

$$D_S \frac{\partial S}{\partial x} \Big|_{x=0} = 0, \quad t > 0, \quad (1.6)$$

Since the substrate diffusivity D_S is finite, the boundary condition 1.6 can be transformed to the following form:

$$\frac{\partial S}{\partial x} \Big|_{x=0} = 0, \quad t > 0, \quad (1.7)$$

Therefore the concentration of the substrate and the product is set constant over the biosensor reaction.

$$S(d,t) = S_0, \quad t > 0, \quad P(d,t) = S_0, \quad t > 0, \quad (1.8a)$$

1.2.3 Dimensionless model

To extract the main governing parameters of the biosensor model with a view to reduce the number of parameters, a dimensionless model is usually created. The parameters x, t of the mathematical model (1.3 - 1.8) and concentrations S and P are replaced by dimensionless parameters:

$$\hat{X} = x/d, \quad \hat{T} = tD_{S_1}/d^2, \quad (1.9a)$$

$$\hat{S} = S/K_M, \quad \hat{P} = P/K_M, \quad (1.9b)$$

where \hat{X} is a dimensionless distance from the electrode, \hat{T} is a dimensionless time, \hat{S} is dimensionless substrate concentration, and \hat{P} is a dimensionless product concentration. Due to dimensionless parameters, governing equation 1.3 is referred to as follows:

$$\frac{\partial \hat{S}}{\partial \hat{T}} = \frac{\partial^2 \hat{S}}{\partial \hat{X}^2} - \alpha^2 \frac{\hat{S}}{1 + \hat{S}}, \quad (1.10a)$$

$$\frac{\partial \hat{P}}{\partial \hat{T}} = \frac{D_P}{D_S} \frac{\partial^2 \hat{P}}{\partial \hat{X}^2} + \alpha^2 \frac{\hat{S}}{1 + \hat{S}}, \quad \hat{X} \in (0, 1), \quad \hat{T} > 0, \quad (1.10b)$$

where α^2 is the diffusion module, also known as a Damköhler number [15],

$$\alpha^2 = \frac{d^2 V_{\max}}{D_S K_M}. \quad (1.11)$$

The diffusion module α^2 compares the rate of the enzyme reaction (V_{\max}/K_M) with the rate of the mass transport through the enzyme layer (D_{S_1}/d^2). A initial conditions for dimensionless model 1.4 are converted in to the following:

$$\hat{P}(\hat{X}, 0) = 0, \quad \hat{S}(\hat{X}, 0) = 0, \quad \hat{X} \in [0, 1), \quad (1.12a)$$

$$\hat{P}(1, 0) = \hat{P}_0, \quad \hat{S}(1, 0) = \hat{S}_0. \quad (1.12b)$$

where \hat{S}_0 and \hat{P}_0 are dimensionless concentrations of substrate and product, respectively.

Dimensionless conditions (1.5 - 1.8) transform in to the following conditions ($\hat{T} > 0$):

$$\hat{P}(0, \hat{T}) = 0, \quad \left. \frac{\partial \hat{S}}{\partial \hat{X}} \right|_{\hat{X}=0} = 0, \quad (1.13a)$$

$$\hat{P}(1, \hat{T}) = \hat{P}_0, \quad \hat{S}(1, \hat{T}) = \hat{S}_0 \quad (1.13b)$$

The diffusion module α^2 is one of the main characteristics of the dimensionless model, expressing internal processes of the biosensor model.

1.3 Numerical biosensor solution

An exact analytical solution is practically possible because of the nonlinearity of the governing equations of the mathematical model 1.3-1.8 [15, 16]. Due to that the initial boundary value problem was solved numerically, when solving the problem, an implicit finite difference scheme was built on a uniform discrete grid [15, 35, 41, 42].

1.3.1 Biosensor current

The current is mainly the most important parameter, measured during or after the reaction. It is a result of the biosensor reaction and is measured on the surface of the electrode.

$$i_A(t) = n_e F A D_P \left. \frac{\partial P}{\partial x} \right|_{x=0}, \quad (1.14)$$

where n_e is the number of electrons involved in the charge transfer, A is the area of the electrode, and F is the Faraday constant, $F = 96.485\text{C/mol}$.

The current is normalized with the area of the surface. The density $i(t)$ of the current at time t is:

$$i(A) = \frac{i_A}{A} = n_e F D_P \left. \frac{\partial P}{\partial x} \right|_{x=0}. \quad (1.15)$$

The system reaches its equilibrium as $t \rightarrow \infty$:

$$I = \lim_{t \rightarrow \infty} i(t). \quad (1.16)$$

The dimensionless model, considering 1.9, dimensionless \hat{I} of the steady state current is set as follows:

$$\hat{i}(\hat{t}) = \left. \frac{\partial \hat{P}}{\partial \hat{x}} \right|_{\hat{x}=0} = \frac{i(t)d}{n_e F D_P K_M}, \quad \hat{I} = \lim_{\hat{t} \rightarrow \infty} \hat{i}(\hat{t}). \quad (1.17)$$

1.3.2 Reaction time of the model

The period from the beginning of the reaction until the time the model is stopped being studied is called the model reaction time. Usually reaction is measured until the current deflection is set smaller than the given value. In the biosensor

model the current is measured till the response reaches the steady-state with an accuracy of the rate ε :

$$T = \min_{i(t) > 0} \left\{ t : \frac{t}{i(t)} \left| \frac{di(t)}{dt} \right| < \varepsilon \right\}. \quad (1.18)$$

where T is the response time. The decay rate *epsilon* influences the reaction time as $T \rightarrow \infty, \varepsilon \rightarrow \infty$

1.3.3 Flow injection analysis

The biosensors are combined with the flow injection analysis (FIA) for on-line monitoring of raw materials, product quality and the manufacturing process [43–45]. In the FIA, a biosensor contacts with the substrate for a short time (seconds to tens of seconds), whereas in the batch analysis the biosensor remains immersed in the substrate solution for a reaction-length time [46]. Biosensors in the flow injection mode are modelled when a single contact with a substrate is considered, and systems are also analyzed when the contact with a substrate is executed with the defined frequency [47–49]. Comparing to the batch systems, the FIA systems present the advantages in reduction of the analysis time allowing a high sample throughput, and the possibility to work with small volumes of the substrate [50–52]. The FIA arrangement also presents a wide response range and a high sensitivity [53, 54].

Actual biosensors, acting in the FIA mode have been already modelled usually at internal diffusion limitations by ignoring the external diffusion [40, 55], although the mechanisms controlling the sensitivity of amperometric biosensors acting in FIA mode can be found, where they were numerically modelled taking into consideration the external mass transport [56]. However, in practical biosensing systems, the mass transport outside the enzyme region is of crucial importance,

and it has to be taken into consideration when modelling the biosensor action [57–59]. The theoretical investigation of the FIA biosensing systems presented a higher quality of the concentration prediction than the corresponding batch systems [40, 60].

With a view to improve the efficiency of the development of a novel biosensor as well as to optimize its configuration, it is of crucial important to model the biosensor action [15, 35, 37, 61, 62].

1.3.4 Biosensor sensitivity

The biosensor operation is analysed with a special emphasis on the conditions under which the biosensor sensitivity can be increased and the calibration curve can be prolonged by changing the injection duration, the permeability of the external diffusion layer, the thickness of the enzyme layer, and the catalytic activity of the enzyme. The half-maximal effective concentration constant and the calibration curve of the biosensor were used as one of the main characteristics of the sensitivity [32, 33, 59, 63, 64]. The numerical simulation was carried out using the finite difference technique [35, 41].

1.3.4.1 Half-maximal effective concentration constant

In the Michaelis-Menten kinetic model [65], the Michaelis constant K_M is an approximation of the enzyme affinity for the substrate, based on the rate constants within the reactions (1.1), $K_M = (k_{-1} + k_2)/k_1$, and it is numerically equivalent to the substrate concentration at which half the maximum rate (C_{50}) of the enzyme-catalyzed reaction is achieved [32, 33].

In the case of biosensors, acting in batch mode and exhibiting the Michaelis-Menten kinetics, the concentration C_{50} is usually called the half maximal ef-

fective concentration constant [64]. Under certain conditions, especially under diffusional limitations to the substrate, the half maximal effective concentration constant C_{50} can differ from K_M for the same catalytic process. The known phenomenon has been subjected to the theoretical modelling, and it has been shown that, under certain conditions, the half-maximal effective concentration constant highly depends on the biosensor geometry [59]. Also, a substantial increase of the Michaelis constant has been shown at restricted diffusion of the substrate through an outer membrane covering an enzyme layer [64]. This result appears to be of a high practical interest, since it enables us to expand the linear dependence of biosensor response on the substrate concentration towards the higher concentrations, under a deep diffusion mode of the biosensor operation, whereas the response time increases not very drastically [64]. This property is especially attractive for biosensors, acting in the FIA mode, because of relatively short their response time [40, 52].

In this research, the half-maximal effective concentration constant C_{50} was accepted as the main characteristic of the sensitivity and of the calibration curve of the amperometric biosensors [32, 33, 64]. The greater value of C_{50} corresponds to a wider range of the linear part of the calibration curve. In the case of the batch analysis, C_{50} is usually defined with respect to the steady-state response. In the FIA, since the biosensor current steadies at zero, the constant C_{50} is defined with respect to the maximal current as the substrate concentration at a half-maximum biosensor activity,

$$C_{50} = \left\{ S_0^* : I_{\max}(S_0^*) = 0.5 \lim_{S_0 \rightarrow \infty} I_{\max}(S_0) \right\}, \quad (1.19)$$

where $I_{\max}(S_0)$ is the maximal density of the biosensor current calculated at the substrate concentration S_0 .

A greater value of the half maximal effective concentration C_{50} corresponds to a longer linear part of the calibration curve [66]. At the substrate concentration

S_0 corresponding to a linear part of the calibration curve ($S_0 < C_{50}$) the dimensionless biosensor sensitivity $B_S(S_0)$ is approximately equal to unity [35]. The concentration C_{50} well characterizes the overall sensitivity of the biosensor.

1.3.4.2 Biot number

The Biot number Bi is another dimensionless parameter, widely used to indicate the internal mass transfer resistance to the external one [35, 67, 68]:

$$Bi = \frac{d/D_{S_1}}{\delta/D_{S_2}} = \frac{D_{S_2}d}{D_{S_1}\delta} = \hat{D}_{21} \frac{d}{\delta}. \quad (1.20)$$

where D_{S_1} and D_{S_2} are diffusion coefficients, and d and δ are the thickness of the enzymatic and diffusion layers, respectively.

1.4 Chapter summary

Various biosensors are often used for detecting different substances like pollutants, microbial load, etc. Biosensors are classified by a bioreceptor and transducer. In a biosensor such as a bioreceptor, an enzyme, antibody, nucleic acid, lectins, hormone, the cell structure or tissue can be used. Enzymes are often used in developing biosensors. Dependent on a transducer, systems can be grouped in to electrochemical which are divided into amperometric and potentiometric ones. In thesis amperometric biosensors are used, they are sensitive and reliable devices providing an opportunity instantly identify relevant biocomponents. Mainly biosensors are used in medicine or food industry.

Mainly the biosensor model involves three regions: the enzyme layer (membrane), where the enzymatic reaction as well as the mass transport by diffusion takes place, a diffusion limiting region, where only the diffusion takes place,

and a convective region. In the enzyme layer we consider the enzyme-catalyzed reaction. The current is a result of the biosensor reaction and is measured on the surface of the electrode, it is mainly the most important parameter, measured during or after the reaction.

In thesis the sensitivity of the biosensor, including batch and flow injection mode, is analysed. Three models of the biosensor were taken, each corresponding different structure and characteristics to be studied.

Chapter 2

Biosensor modelling

2.1 Amperometric biosensors in flow injection analysis systems

This research investigates the sensitivity of an amperometric biosensor, acting in the flow injection mode, when the biosensor contacts an analyte for a short time. The analytical system is modelled by non-stationary reaction-diffusion equations, containing a nonlinear term related to the Michaelis-Menten kinetics of an enzymatic reaction [35, 41]. The mathematical model involves three regions: the enzyme layer, where the enzymatic reaction as well as the mass transport by diffusion takes place, a diffusion limiting region, where only the diffusion takes place, and a convective region. The biosensor operation is analysed with a special emphasis on the conditions under which the biosensor sensitivity can be increased and the calibration curve can be prolonged by changing the injection duration, the permeability of the external diffusion layer, the thickness of the enzyme layer and the catalytic activity of the enzyme. The half-maximal effective concentration constant is used as the main characteristic

of the sensitivity and the calibration curve of the biosensor [32, 33, 59, 63, 64].

2.1.1 Mathematical model

The amperometric biosensor is considered as an electrode and a relatively thin layer of an enzyme (enzyme membrane) applied onto the electrode surface. The biosensor model involves three regions: the enzyme layer (membrane) where the enzymatic reaction as well as the mass transport by diffusion takes place, a diffusion limiting region, where only the diffusion takes place, and a convective region (1.1) [32, 33]. Due to the quasi steady-state approximation substrate combines with enzyme resulting the product and enzyme (1.2) [19, 33, 34].

2.1.2 Governing equations

Due to the symmetrical geometry of the electrode and a homogeneous distribution of the immobilized enzyme in the enzyme layer of a uniform thickness, the mathematical model of the biosensor action can be defined in a one-dimensional-in-space domain [15, 16, 35]. Coupling the enzyme catalyzed reaction (1.2) in the enzyme layer with the mass transport by diffusion, described by Fick's law, leads to the following system of the reaction diffusion equations:

$$\frac{\partial S_1}{\partial t} = D_{S_1} \frac{\partial^2 S_1}{\partial x^2} - \frac{V_{\max} S_1}{K_M + S_1}, \quad (2.1a)$$

$$\frac{\partial P_1}{\partial t} = D_{P_1} \frac{\partial^2 P_1}{\partial x^2} + \frac{V_{\max} S_1}{K_M + S_1}, \quad x \in (0, d), \quad t > 0, \quad (2.1b)$$

where x and t denote a space and time, S_1 and P_1 are the concentrations of the substrate (S) and product (P) in the enzyme layer, D_{S_1} , D_{P_1} are the diffusion coefficients, V_{\max} is the maximal enzymatic rate attainable with that amount of the enzyme, when the enzyme is fully saturated with the substrate, K_M is the

Michaelis constant, and d is the thickness of the enzyme layer [15, 36, 37]. The Michaelis constant K_M is the concentration of the substrate at which the reaction rate is half its maximum value V_{\max} .

In the outer layer, only the mass transport by diffusion of both species takes place. We assume that the outer mass transport obeys the finite diffusion regime,

$$\frac{\partial S_2}{\partial t} = D_{S_2} \frac{\partial^2 S_2}{\partial x^2}, \quad (2.2a)$$

$$\frac{\partial P_2}{\partial t} = D_{P_2} \frac{\partial^2 P_2}{\partial x^2}, \quad x \in (d, d + \delta), \quad t > 0, \quad (2.2b)$$

where S_2 and P_2 are the substrate and product concentrations in the outer layer, D_{S_2} and D_{P_2} are the diffusion coefficients, and δ is the thickness of the diffusion layer.

2.1.3 Initial and boundary conditions

Let $x = 0$ represent the surface of the electrode, while $x = d + \delta$ is a farther boundary of the diffusion layer. The biosensor operation starts, when the substrate appears in the bulk solution ($t = 0$),

$$P_1(x, 0) = 0, \quad S_1(x, 0) = 0, \quad x \in [0, d], \quad (2.3a)$$

$$P_2(x, 0) = 0, \quad x \in [d, d + \delta], \quad (2.3b)$$

$$S_2(x, 0) = \begin{cases} 0, & x \in [d, d + \delta), \\ S_0, & x = d + \delta, \end{cases} \quad (2.3c)$$

where S_0 is the substrate concentration in the bulk solution.

During the biosensor operation, the substrate penetrates through the diffusion layer and reaches the farthest boundary of the enzyme layer ($x = d$), where we

define the matching conditions ($t > 0$):

$$D_{S_1} \frac{\partial S_1}{\partial x} \Big|_{x=d} = D_{S_2} \frac{\partial S_2}{\partial x} \Big|_{x=d}, \quad S_1(d, t) = S_2(d, t), \quad (2.4a)$$

$$D_{P_1} \frac{\partial P_1}{\partial x} \Big|_{x=d} = D_{P_2} \frac{\partial P_2}{\partial x} \Big|_{x=d}, \quad P_1(d, t) = P_2(d, t). \quad (2.4b)$$

It is shown by these conditions that the amount of the substrate, which has penetrated through the diffusion layer, enters the enzyme membrane.

Due to the electrode polarization, the concentration of the reaction product at the electrode surface is permanently reduced to zero [15, 35]. The substrate concentration flux on the electrode surface equals zero because of the substrate electro-inactivity,

$$P_1(0, t) = 0, \quad \frac{\partial S_1}{\partial x} \Big|_{x=0} = 0. \quad (2.5)$$

The outer diffusion layer ($d < x < d + \delta$) is treated as the Nernst diffusion layer [41]. According to the Nernst approach, the layer of the thickness δ remains unchanged with time, and away from it the solution is uniform in the concentration ($t > 0$). In the FIA mode of the biosensor operation, the substrate appears in the bulk solution only for a short time period, called the injection time. Later, the substrate disappears from the bulk solution,

$$P_2(d + \delta, t) = 0, \quad S_2(d + \delta, t) = \begin{cases} S_0, & t \leq T_F, \\ 0, & t > T_F, \end{cases} \quad (2.6)$$

where T_F is the injection time.

2.1.4 Biosensor response

The anodic or cathodic current is measured as a result of a physical experiment. The current is proportional to the gradient of the reaction product concentration

at the electrode surface, i.e. on the border $x = 0$. The density $I(t)$ of the biosensor current at time t can be obtained explicitly from Faraday's and Fick's laws [15],

$$I(t) = n_e F D_{P_1} \left. \frac{\partial P_1}{\partial x} \right|_{x=0}, \quad (2.7)$$

where n_e is the number of electrons involved in a charge transfer, and F is the Faraday constant.

We assume that the system reaches the equilibrium as $t \rightarrow \infty$. The steady-state current is the main characteristic in commercial amperometric biosensors acting in the batch mode [19, 32, 33]. In FIA, due to the zero concentration of the surrounding substrate at $t > T_F$, the steady-state current falls to zero, $I(t) \rightarrow 0$, as $t \rightarrow \infty$. Because of this, the steady-state current is not practically useful in the FIA systems. Since the current density $I(t)$ of the biosensor acting in the injection mode, is a non-monotonous function, the maximal current is one of the mostly used characteristics for this kind of biosensors,

$$I_{\max} = \max_{t>0} \{I(t)\}, \quad (2.8)$$

where I_{\max} is the maximal density of the biosensor current.

2.1.5 Dimensionless model

In order to define the main governing parameters of the mathematical model, thus reducing the number of model parameters in general, a dimensionless model is often derived [15, 61, 67]. For simplicity, we introduce the concentrations S and P of the substrate and the product for the entire domain $x \in [0, d + \delta]$ ($t \geq 0$),

$$S = \begin{cases} S_1, & 0 \leq x \leq d, \\ S_2, & d < x \leq d + \delta, \end{cases} \quad (2.9a)$$

$$P = \begin{cases} P_1, & 0 \leq x \leq d, \\ P_2, & d < x \leq d + \delta. \end{cases} \quad (2.9b)$$

Both concentration functions (S and P) are continuous in the entire domain $x \in [0, d + \delta]$. The replacement of the parameters is based on parameter mappings defined in Table 2.1.

Table 2.1: Dimensional and dimensionless model parameters

| Parameter | Dimensional | Dimensionless |
|--------------------------------------|------------------------------------|---|
| Distance from the electrode | x , cm | $\hat{X} = x/d$ |
| Time | t , s | $\hat{T} = tD_{S_1}/d^2$ |
| Injection time | T_F , s | $\hat{T}_F = T_FD_{S_1}/d^2$ |
| Enzyme layer thickness | d , cm | $\hat{X} = d/d = 1$ |
| Diffusion layer thickness | δ , cm | $\hat{\Delta} = \delta/d$ |
| Substrate concentration | S, S_0 , M | $\hat{S} = S/K_M, \hat{S}_0 = S_0/K_M$ |
| Product concentration | P , M | $\hat{P} = P/K_M$ |
| Half maximal effective concentration | K_M, C_{50} , M | $\hat{K}_M = K_M/K_M = 1, \hat{C}_{50} = C_{50}/K_M$ |
| Current density | I, I_{\max} , A cm ⁻² | $\hat{I} = Id/(n_eFD_{P_1}K_M),$ $\hat{I}_{\max} = I_{\max}d/(n_eFD_{P_1}K_M)$ |

For the enzyme layer, reaction-diffusion equations (2.1) can be rewritten as follows:

$$\frac{\partial \hat{S}}{\partial \hat{T}} = \frac{\partial^2 \hat{S}}{\partial \hat{X}^2} - \alpha^2 \frac{\hat{S}}{1 + \hat{S}}, \quad (2.10a)$$

$$\frac{\partial \hat{P}}{\partial \hat{T}} = \frac{D_{P_1}}{D_{S_1}} \frac{\partial^2 \hat{P}}{\partial \hat{X}^2} + \alpha^2 \frac{\hat{S}}{1 + \hat{S}}, \quad \hat{X} \in (0, 1), \quad \hat{T} > 0, \quad (2.10b)$$

where α^2 is the diffusion module, known as a Damköhler number [15],

$$\alpha^2 = \frac{d^2 V_{\max}}{D_{S_1} K_M}. \quad (2.11)$$

The diffusion module α^2 compares the rate of the enzyme reaction (V_{\max}/K_M) with the rate of the mass transport through the enzyme layer (D_S/d^2).

Diffusion equations (2.2) are transformed as follows:

$$\frac{\partial \hat{S}}{\partial \hat{T}} = \frac{D_{S_2}}{D_{S_1}} \frac{\partial^2 \hat{S}}{\partial \hat{X}^2}, \quad (2.12a)$$

$$\frac{\partial \hat{P}}{\partial \hat{T}} = \frac{D_{P_2}}{D_{S_1}} \frac{\partial^2 \hat{P}}{\partial \hat{X}^2}, \quad \hat{X} \in (1, 1 + \hat{\Delta}), \quad \hat{T} > 0. \quad (2.12b)$$

The initial conditions (2.3) take the following form:

$$\hat{P}(\hat{X}, 0) = 0, \quad \hat{S}(\hat{X}, 0) = 0, \quad \hat{X} \in [0, 1 + \hat{\Delta}], \quad (2.13a)$$

$$\hat{P}(1 + \hat{\Delta}, 0) = 0, \quad \hat{S}(1 + \hat{\Delta}, 0) = \hat{S}_0. \quad (2.13b)$$

The matching conditions (2.4) transform to the following conditions ($\hat{T} > 0$):

$$\left. \frac{\partial \hat{S}}{\partial \hat{X}} \right|_{\hat{X}=1} = \frac{D_{S_2}}{D_{S_1}} \left. \frac{\partial \hat{S}}{\partial \hat{X}} \right|_{\hat{X}=1}, \quad (2.14a)$$

$$\left. \frac{D_{P_1}}{D_{S_1}} \frac{\partial \hat{P}}{\partial \hat{X}} \right|_{\hat{X}=1} = \left. \frac{D_{P_2}}{D_{S_1}} \frac{\partial \hat{P}}{\partial \hat{X}} \right|_{\hat{X}=1}. \quad (2.14b)$$

Boundary conditions (2.5) and (2.6) acquire the following form ($\hat{T} > 0$):

$$\hat{P}(0, \hat{T}) = 0, \quad \left. \frac{\partial \hat{S}}{\partial \hat{X}} \right|_{\hat{X}=0} = 0, \quad (2.15a)$$

$$\hat{P}(1 + \hat{\Delta}, \hat{T}) = 0, \quad \hat{S}(1 + \hat{\Delta}, \hat{T}) = \begin{cases} \hat{S}_0, & \hat{T} \leq \hat{T}_F, \\ 0, & \hat{T} > \hat{T}_F. \end{cases} \quad (2.15b)$$

The dimensionless current (flux) \hat{I} is defined as follows:

$$\hat{I}(\hat{T}) = \left. \frac{\partial \hat{P}}{\partial \hat{X}} \right|_{\hat{X}=0} = \frac{I(t)d}{n_e F D_{P_1} K_M}. \quad (2.16)$$

Due to the same diffusion coefficients of both species considered, the substrate and the product, the initial collection of model parameters reduces to a few aggregate parameters: $\hat{\Delta}$ is the diffusion layer thickness, α^2 is the diffusion module, \hat{T}_F is the injection time, \hat{S}_0 is the substrate concentration in the bulk during the injection, and $\hat{D}_{21} = D_{S_2}/D_{S_1} = D_{P_2}/D_{P_1}$ is the dimensionless ratio of the diffusion coefficient in the diffusion layer to the corresponding diffusion coefficient in the enzyme layer. The diffusion module α^2 is one of the most important parameters that essentially define internal characteristics of an amperometric biosensor [15, 35–37]. The biosensor response is known to be under diffusion control as $\alpha^2 \gg 1$. In the very opposite case, where $\alpha^2 \ll 1$, the enzyme kinetics predominates in the response.

2.1.6 Numerical simulation

No analytical solution is possible because of the nonlinearity of governing equations of the mathematical model (2.1)-(2.7) [15, 16]. For this reason a numerical solution was performed. When solving the biosensor model, an implicit finite difference scheme has been formed on a uniform discrete grid [15, 35, 41, 42].

The mathematical model and the numerical solution were validated using the known analytical solution [15]. Assuming $T_F \rightarrow \infty$, the mathematical model (2.1)-(2.7) approaches the two-compartment model of the amperometric biosensor, acting in the batch mode [15]. In addition, assuming $S_0 \ll K_M$, the nonlinear reaction (Michaelis-Menten) function in (2.1) simplifies to a linear function $V_{\max}S_1/K_M$. Based on these assumptions model (2.1)-(2.7) has been analytically solved under the steady-state conditions [15].

A number of experiments were done, while the values of some parameters were

kept constant [69],

$$\begin{aligned} D_{S_1} = D_{P_1} = 300 \mu\text{m}^2/\text{s}, \quad D_{S_2} = 2D_{S_1}, \quad D_{P_2} = 2D_{P_1}, \\ K_M = 100 \mu\text{M}, \quad n_e = 1, \quad d = 200 \mu\text{m}. \end{aligned} \quad (2.17)$$

Fig. 2.1 shows the evolution of the density $I(t)$ of the biosensor current. The biosensor action was simulated at a moderate concentration S_0 of the substrate ($S_0 = K_M$) and different values of the other model parameters, the dimensionless diffusion module α^2 (1 and 2), the injection time T_F (3 and 6 s) and the dimensionless Biot number Bi (1 and 2). Assuming (2.17), these two values (1 and 2) of α^2 have been obtained with the following values of the maximal enzymatic rate V_{max} : 0.75 and 1.5 μM , respectively. Accordingly, $Bi = 2$ corresponds to the thickness δ of the external diffusion layer equal to the thickness d of the enzyme layer, while $Bi = 1$ as $\delta = \hat{D}_{21}d = 2d = 400 \mu\text{m}$.

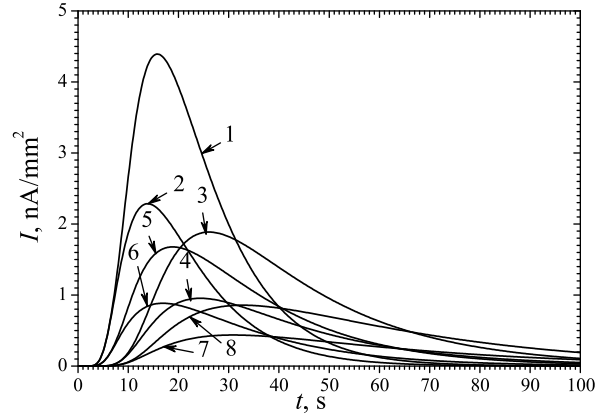


Figure 2.1: The dynamics of the biosensor response at different values of the diffusion module α^2 : 1 (5-8), 2 (1-4), the Biot number Bi : 1 (3, 4, 7, 8), 2 (1, 2, 5, 6) and the injection time T_F : 3 (2, 4, 6, 8), 6 s (1, 3, 5, 7)

One can see in Fig. 2.1 the non-monotonous behaviour of the biosensor current. In all the cases the current increases during the injection period ($t \leq T_F$). However, the current also increases some time after the substrate disappearance from the bulk solution ($t \geq T_F$). The time moment of the maximum current as well

as the maximal current itself depend on all the three model parameters: α^2 , Bi , and T_F .

Fig. 2.1 shows that the density I_{\max} of the maximal current increases almost two times when the injection time T_F doubles. However, the influence of the doubling the time T_F on the time of the maximal current is rather slight. When comparing curves 1 ($T_F = 6$) and 2 ($T_F = 3$ s), one can see that the time of the maximal response increases from 13.9 only to 16 s, while I_{\max} increases from 2.3 event to 4.4 nA/mm² as $\alpha^2 = 2$, $Bi = 2$.

Fig. 2.1 also shows that the biosensor response significantly depends on the Biot number Bi . A decrease in Bi noticeably prolongs the response. As one can see in Fig. 2.1, the maximal current decreases when the thickness of the external diffusion layer increases, i.e. Bi decreases. FIA biosensing systems have been already investigated by using mathematical models at zero thickness ($Bi \rightarrow \infty$) of the external diffusion layer [40, 60]. Fig. 2.1 visually substantiates the importance of the external diffusion layer.

2.1.7 Results and discussion

Using the numerical simulation, the biosensor operation was analysed with a special emphasis on the conditions under which the biosensor sensitivity can be increased and the calibration curve can be prolonged by changing the injection duration, the biosensor geometry, and the catalytic activity of the enzyme. In order to investigate the influence of the model parameters on the half-maximal effective concentration constant \hat{C}_{50} , the simulation was performed within a wide range of the values of the diffusion module α^2 , the Biot number Bi and the injection time T_F . Since in the FIA, the injection usually continues for several seconds (neither minutes, nor milliseconds), to render the injection time more lucidly, we used the dimensional injection time T_F instead of the dimensionless

injection time \hat{T}_F .

The constant \hat{C}_{50} expresses a relative prolongation (in times) of the calibration curve in comparison with the theoretical Michaelis constant K_M . For a biosensor of concrete configuration, \hat{C}_{50} can be rather easily calculated by multiple simulation of the maximal response, changing the substrate concentration \hat{S}_0 .

Fig. 2.2 shows the dependence of the half-maximal effective concentration constant \hat{C}_{50} on the Biot number Bi . The constant \hat{C}_{50} was calculated with three values of the diffusion module α^2 : 0.1 (curves 1 and 2), 1 (3, 4) and 10 (5, 6), and two practically extreme values of the injection time T_F : 1 (1, 3, 5) and 10 s (2, 4, 6). At concrete values of α^2 and T_F , the calculations were performed by changing the thickness δ of the diffusion layer from $40\ \mu\text{m}$ ($\delta = 0.2d$) to $4\ \text{mm}$ ($\delta = 20d$) and keeping constant the thickness $d = 200\ \mu\text{m}$ of the enzyme layer.

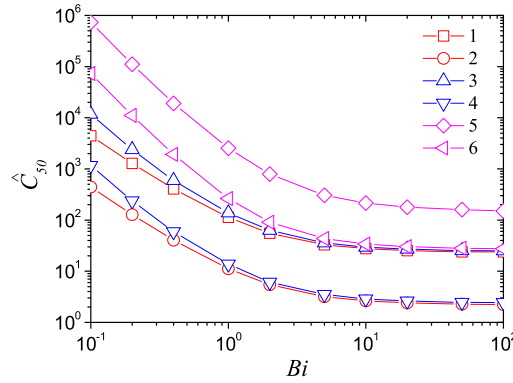


Figure 2.2: The dependence of the half-maximal effective concentration constant \hat{C}_{50} on the Biot number Bi with different values of the diffusion module α^2 : 0.1 (1, 2), 1 (3, 4), 10 (5, 6) and the injection time T_F : 1 (1, 3, 5), 10 s (2, 4, 6)

One can see in Fig. 2.2, that at relatively large values of the Biot number ($Bi > 10$) the half-maximal effective concentration constant \hat{C}_{50} (as well as dimensional C_{50}) is almost insensitive to changes in Bi . However, when $Bi < 1$, a decrease in Bi affects a drastic increase of \hat{C}_{50} . By increasing the thickness δ of the external diffusion layer as well as decreasing the diffusivity D_{S_2} in this layer, i.e. by

decreasing Bi , the calibration curve of the biosensor can be prolonged by a few orders of magnitude. The diffusivity of species in the diffusion layer is usually relative to the permeability of the diffusion layer. The Biot number Bi might be also decreased by decreasing the permeability of the external diffusion layer.

In the case of the batch analysis, an advantageous effect of the external diffusivity on the length of the calibration curve of amperometric biosensors is quite well known [32, 33, 59, 64]. Fig. 2.2 shows that, due to FIA, the linear part of the calibration curve becomes even longer. This figure also shows a weak dependence of \hat{C}_{50} on the diffusion module α^2 as $\alpha^2 \leq 1$.

To properly investigate the impact of the injection time T_F on the length of the linear part of the calibration curve, the half-maximal effective concentration constant \hat{C}_{50} was calculated by changing T_F from 1 up to 10 s. The values of \hat{C}_{50} were calculated with three values of the diffusion module α^2 (0.1, 1 and 10) and three values of the Biot number Bi (0.1, 10 and 100). The calculation results are depicted in Fig. 2.3.

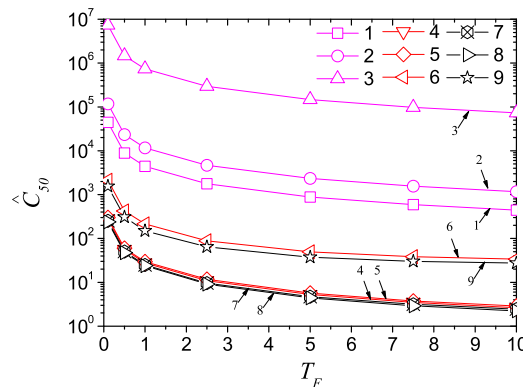


Figure 2.3: The half maximal effective concentration constant \hat{C}_{50} vs. the injection time T_F , α^2 : 0.1 (1, 4, 7), 1 (2, 5, 8), 10 (3, 6, 9), Bi : 0.1 (1-3), 10 (4-6), 100 (7-9)

As one can see in Fig. 2.3, \hat{C}_{50} exponentially increases with a decrease in the injection time T_F . The calibration curve of the biosensor can be prolonged by a

few orders of magnitude only by decreasing the injection time T_F . The impact of T_F is practically invariant for the Biot number Bi and the diffusion module α^2 . The exponential increase is specifically characteristic at low values of T_F ($T_F < 3$ s).

In Fig. 2.3 one can also see no noticeable difference between curves 4, 5, 7, and 8. Two other curves, 6 and 9, only slightly differ from each other. So, at relatively high values of the Biot number ($Bi \geq 10$), \hat{C}_{50} is but slightly sensitive to changes in Bi . This effect was even more easily shown in Fig. 2.2. Fig. 2.3 additionally shows that the \hat{C}_{50} more increases at greater values of the diffusion module α^2 rather than at lower ones.

Finally, the impact of the diffusion module α^2 on the half-maximal effective concentration constant has been evaluated. The result is presented in Fig. 2.4. The constant \hat{C}_{50} was calculated for three values of the diffusion Biot number Bi : 0.1 (curves 1 and 4), 10 (2, 5) and 100 (3, 6), and two values of the injection time T_F : 1 (1-3) and 10 s (4-6). At concrete values of Bi and T_F , the calculations were performed by changing the maximal enzymatic rate V_{\max} from 75 nM/s ($\alpha^2 = 0.1$) to 7.5 μ M/s ($\alpha^2 = 10$) and keeping other parameters constant.

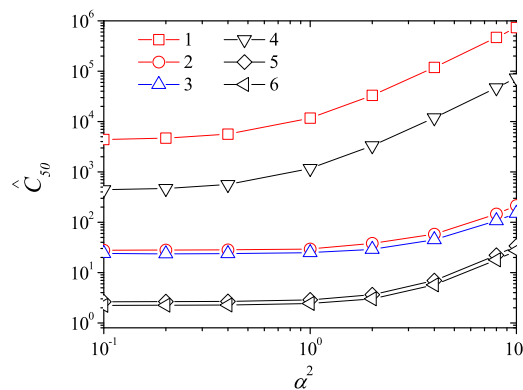


Figure 2.4: The half maximal effective concentration constant \hat{C}_{50} vs. the diffusion module α^2 , Bi : 0.1 (1, 4), 10 (2, 5), 100 (3, 6), T_F : 1 (1-3), 10 s (4-6)

As one can see in Fig. 2.4, \hat{C}_{50} is a monotonous increasing function of α^2 . When the enzyme kinetics predominates in response ($\alpha^2 < 1$) of a FIA biosensing system with a relatively large Biot number ($Bi \geq 10$), the \hat{C}_{50} is approximately a constant function (curves 2, 3, 5 and 6). When the biosensor response is under diffusion control ($\alpha^2 > 1$), \hat{C}_{50} exponentially increases with an increase in the diffusion module α^2 . These features were particularly noticed in Fig. 2.2 and Fig. 2.3.

In real applications of biosensors, the diffusion module α^2 can be modified by changing the enzyme activity (V_{\max}) as well as the thickness d of the enzyme layer. The maximal enzymatic rate V_{\max} is actually a product of two parameters: the catalytic constant k_2 and the total concentration E_t of the enzyme [32, 33]. It is usually impossible to modify the k_2 part. The maximal rate V_{\max} might be modified by changing the enzyme concentration E_t in the enzyme layer. V_{\max} is relative to the total enzyme used in a biosensor.

In the batch analysis ($T_F \rightarrow \infty$), where the enzyme kinetics distinctly predominates in the biosensor response ($\alpha^2 \ll 1$ and $Bi \rightarrow \infty$), the half-maximal effective concentration constant C_{50} approaches the theoretical Michaelis constant K_M , i.e. $C_{50} \approx K_M$, $\hat{C}_{50} \approx 1$ [32, 33, 59, 63, 64]. As one can see in Fig. 2.2, Fig. 2.3, and Fig. 2.4, \hat{C}_{50} is quite near to 1 also in the case of the FIA biosensing systems as $\alpha^2 < 1$, $T_F = 10$ and $Bi = 100$.

2.1.8 Section summary

The mathematical model (2.1)-(2.7) of the flow injection analysis system, based on an amperometric biosensor, can be successfully used to investigate the kinetic peculiarities of biosensor response. The respective dimensionless mathematical model (2.10)-(2.35) can be used as a framework for numerical investigation of the impact of model parameters on the biosensor action and to optimize the

biosensor configuration.

By increasing the thickness δ of the external diffusion layer or by decreasing the substrate diffusivity D_{S_2} in this layer (by decreasing the Biot number Bi), the calibration curve of the biosensor can be prolonged by a few orders of magnitude. At relatively large values of the Biot number ($Bi > 10$) the half-maximal effective concentration constant C_{50} is almost insensitive to changes in Bi Fig. 2.2.

The half-maximal effective concentration constant C_{50} exponentially increases with a decrease in the injection time T_F . The calibration curve of the biosensor can be prolonged by a few orders of magnitude only by decreasing the injection time T_F . The impact of T_F is practically invariant on the Biot number Bi and the diffusion module α^2 . The exponential increase is specifically characteristic at low values of T_F ($T_F < 3$ s) Fig. 2.3.

C_{50} is a monotonously increasing function of the diffusion module α^2 . When the enzyme kinetics distinctly predominates in the response ($\alpha^2 < 1$ and $Bi \geq 10$), C_{50} is approximately a constant function, while as $\alpha^2 > 1$ C_{50} exponentially increases with an increase in α^2 Fig. 2.4.

2.2 Modelling and simulation of amperometric biosensors acting in the flow injection analysis

The goal of this investigation was to develop a computational model for an effective simulation of the action of an amperometric biosensor that contains dialysis membranes and utilizes FIA, as well as to investigate the influence of the physical and kinetic parameters on the biosensor response. The biosensing system was mathematically modelled by reaction-diffusion equations that include a nonlinear term related to the Michaelis-Menten kinetics of the enzymatic

reaction [15, 37]. The system of equations was solved numerically by using the finite difference technique [35, 41]. The biosensor operation was analyzed especially emphasizing on the effect of the dialysis membrane on the biosensor response. The biosensor sensitivity was investigated by altering the model parameters that influence the thickness of the dialysis membrane and the catalytic activity of the enzyme. The half-maximal effective concentration of the analyte was used as the base characteristic of sensitivity and the calibration curve of the biosensor [66].

2.2.1 Biosensor structure

The biosensor to be modelled has a layered structure [70]. Fig. 2.5 shows a principal structure of the biosensor. The biosensor is considered as an electrode with a relatively thin layer of an enzyme (enzyme membrane) entrapped on the surface of the electrode applying the dialysis membrane. The biosensor model involves four regions: the enzyme layer where the enzyme reaction as well as the mass transport by diffusion takes place, a dialysis membrane and a diffusion limiting region where only the mass transport by diffusion take place, and a convective region where the analyte concentration is maintained constant.

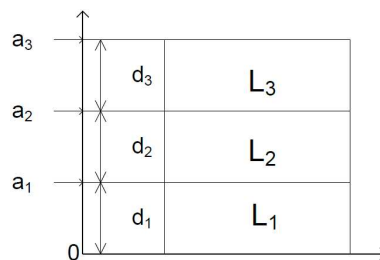


Figure 2.5: Structural Scheme of the Biosensor

In the enzyme layer, we consider the enzyme-catalyzed reaction, where the product is created as a result (1.1). The complex then dissociates into the product (P) and the enzyme is regenerated [32, 33].

Due to the quasi steady-state approximation, the concentration of the intermediate complex (ES) does not change and may be neglected when modelling the biochemical behaviour of biosensors [33, 34, 71]. In the resulting scheme (1.2), the substrate (S) is enzymatically converted in to the product (P).

It was assumed that $x = 0$ represents the surface of the electrode, a_1 , a_2 , and a_3 denote the distances from the electrode surface, while d_1 , d_2 , and d_3 are thicknesses of the enzyme, the dialysis membrane, and the diffusion layers, respectively, $a_i = a_{i-1} + d_i$, $i = 1, 2, 3$, and $a_0 = 0$. The outer diffusion layer ($a_2 < x < a_3$) may be treated as the Nernst diffusion layer [41]. According to the Nernst approach, the layer of thickness $d_3 = a_3 - a_2$ remains unchanged with time. It was assumed that away from it the buffer solution is uniform in the concentration.

2.2.2 Mathematical model

Due to a homogeneous distribution of the enzyme in the enzyme layer of the uniform thickness and symmetrical geometry of the dialysis membrane leads to a mathematical model of the biosensor action defined in a one-dimensional-in-space domain [15, 35].

2.2.3 Governing equations

Coupling the enzyme-catalyzed reaction (1.2) in the enzyme layer with the mass transport by diffusion, described by Fick's law, leads to the following system of

the reaction-diffusion equations ($t > 0$):

$$\frac{\partial S_1}{\partial t} = D_{S_1} \frac{\partial^2 S_1}{\partial x^2} - \frac{V_{\max} S_1}{K_M + S_1}, \quad (2.18a)$$

$$\frac{\partial P_1}{\partial t} = D_{P_1} \frac{\partial^2 P_1}{\partial x^2} + \frac{V_{\max} S_1}{K_M + S_1}, \quad x \in (0, a_1), \quad (2.18b)$$

where x and t stand for space and time, S_1 and P_1 are concentrations of the substrate (S) and the product (P) in the enzyme layer, D_{S_1} , D_{P_1} are the constant diffusion coefficients, V_{\max} is the maximal enzymatic rate attainable with that amount of the enzyme, if the enzyme is fully saturated with the substrate, K_M is the Michaelis constant, and $d_1 = a_1$ is the thickness of the enzyme layer [15, 36, 37]. The Michaelis constant K_M is the concentration of the substrate (S) at which the reaction rate is half its maximum value V_{\max} . K_M is an approximation of the enzyme affinity to the substrate based on the rate constants within the reactions (1.1), $K_M = (k_{-1} + k_2)/k_1$.

Outside the enzyme layer, only the mass transport by diffusion of the substrate as well as the product takes place ($t > 0$),

$$\frac{\partial S_i}{\partial t} = D_{S_i} \frac{\partial^2 S_i}{\partial x^2}, \quad (2.19a)$$

$$\frac{\partial P_i}{\partial t} = D_{P_i} \frac{\partial^2 P_i}{\partial x^2}, \quad x \in (a_{i-1}, a_i), \quad i = 2, 3, \quad (2.19b)$$

where S_i and P_i are the substrate and the product concentrations in the i -th layer, D_{S_i} and D_{P_i} are the diffusion coefficients, and $d_i = a_i - a_{i-1}$ is the thickness of the corresponding layer, $i = 2, 3$.

2.2.4 Initial conditions

The biosensor operation starts when a substrate appears in the bulk solution. It leads to the following initial conditions ($t = 0$):

$$S_1(x, 0) = 0, \quad P_1(x, 0) = 0, \quad x \in [0, a_1], \quad (2.20a)$$

$$S_2(x, 0) = 0, \quad P_2(x, 0) = 0, \quad x \in [a_1, a_2], \quad (2.20b)$$

$$S_3(x, 0) = \begin{cases} 0, & x \in [a_2, a_3), \\ S_0, & x = a_3, \end{cases} \quad (2.20c)$$

$$P_3(x, 0) = 0, \quad x \in [a_2, a_3], \quad (2.20d)$$

where S_0 is the substrate concentration in the bulk solution.

2.2.5 Boundary conditions

During the biosensor operation, the substrate penetrates through the diffusion layer as well as the dialysis membrane and reaches a farther boundary of the enzyme layer ($x = a_1$). On the boundary between two adjacent regions with different diffusivities, the matching conditions have to be defined ($t > 0, i = 1, 2$):

$$D_{S_i} \frac{\partial S_i}{\partial x} \Big|_{x=a_i} = D_{S_{i+1}} \frac{\partial S_{i+1}}{\partial x} \Big|_{x=a_i}, \quad (2.21a)$$

$$S_i(a_i, t) = S_{i+1}(a_i, t), \quad (2.21b)$$

$$D_{P_i} \frac{\partial P_i}{\partial x} \Big|_{x=a_i} = D_{P_{i+1}} \frac{\partial P_{i+1}}{\partial x} \Big|_{x=a_i}, \quad (2.21c)$$

$$P_i(a_i, t) = P_{i+1}(a_i, t). \quad (2.21d)$$

These conditions mean that fluxes of the substrate and the product through one region are equal to the respective fluxes, entering the surface of the neighbouring

region. Concentrations of the substrate and the product in one region versus the neighbouring region are assumed to be equal.

Due to the electrode polarization, the concentration of the reaction product at the electrode surface is permanently reduced to zero [15, 35],

$$P_1(0, t) = 0, \quad (2.22)$$

Due to the substrate electro-inactivity, the substrate concentration flux on the electrode surface equals zero,

$$\left. \frac{\partial S_1}{\partial x} \right|_{x=0} = 0. \quad (2.23)$$

According to the Nernst approach, the layer of the thickness d_3 of the outer diffusion layer remains unchanged with time, and away from it the solution is uniform in the concentration [41]. In the FIA mode of the biosensor operation, the substrate appears in the bulk solution only for a short time period called the injection time [72]. Later, the substrate disappears from the bulk solution,

$$P_3(a_3, t) = 0, \quad t > 0, \quad (2.24a)$$

$$S_3(a_3, t) = \begin{cases} S_0, & 0 < t \leq T_F, \\ 0, & t > T_F, \end{cases} \quad (2.24b)$$

where T_F is the injection time.

2.2.6 Biosensor response

The anodic or cathodic current is measured as a result in a physical experiment. The biosensor current is proportional to the gradient of the reaction product concentration at the electrode surface, i.e. on the boundary $x = 0$. When modelling

the biosensor action, due to the direct proportionality of the current to the area of the electrode surface, the current is often normalized with that area [15, 35]. The density $I(t)$ of the biosensor current at time t can be obtained explicitly from Faraday's and Fick's laws [15],

$$I(t) = n_e F D_{P_1} \left. \frac{\partial P_1}{\partial x} \right|_{x=0}, \quad (2.25)$$

where n_e is the number of electrons involved in charge transfer, and F is the Faraday constant.

We assume that the system achieves an equilibrium as $t \rightarrow \infty$. The steady-state current is usually assumed to be the main characteristic of commercial amperometric biosensors acting in the batch mode [32, 33, 71]. In FIA, due to the zero concentration of the surrounding substrate at $t > T_F$, the steady-state current falls to zero, $I(t) \rightarrow 0$, as $t \rightarrow \infty$. Because of this, the maximum peak current is the most often used characteristic in FIA systems,

$$I_{\max} = \max_{t>0} \{I(t)\}, \quad (2.26)$$

where I_{\max} is the maximal density of the biosensor current.

The corresponding time T_{\max} of the maximal current is used to characterize the response time of the biosensor,

$$T_{\max} = \{t : I(t) = I_{\max}\}. \quad (2.27)$$

2.2.7 Characteristics of Biosensor Response

Sensitivity is one of the most important characteristics of the biosensor operation [32, 33, 71]. The sensitivity B_S of the biosensor, acting in the FIA mode, is defined as the gradient of the maximal current with respect to the concentration

S_0 of the substrate in the bulk [15, 35]. Since the biosensor current as well as the substrate concentration vary even in orders of magnitude, a dimensionless expression of sensitivity is preferable [35]. The dimensionless sensitivity $B_S(S_0)$ for the substrate concentration S_0 is given by

$$B_S(S_0) = \frac{dI_{\max}(S_0)}{dS_0} \times \frac{S_0}{I_{\max}(S_0)}, \quad (2.28)$$

where $I_{\max}(S_0)$ is the density of the maximal biosensor current, calculated at the substrate concentration S_0 .

In the Michaelis-Menten kinetic model, the Michaelis constant K_M as a characteristic of the biosensor calibration curve is numerically equal to the substrate concentration at which half the maximum rate of the enzyme-catalyzed reaction is achieved [32, 33]. Under certain conditions, especially under diffusion limitations for the substrate, the half-maximal effective concentration C_{50} of the substrate to be determined is often used to characterize the biosensor calibration curve [66]. In the case of FIA analysis, C_{50} is defined as the concentration of the substrate at which the response of the biosensor achieves half the maximal response (1.19).

2.2.8 Dimensionless Model

In order to extract the main governing parameters of the mathematical model, thus reducing the number of model parameters in general, a dimensionless model is often derived [15, 61]. The dimensionless model has been derived by replacing the model parameters as defined in the following table:

For the enzyme layer, the reaction-diffusion equations (2.18) can be rewritten as

Table 2.2: Dimensional and dimensionless model parameters ($i = 1, 2, 3$)

| Dimensional | Dimensionless |
|--------------------------------|-------------------------------------|
| x , cm | $\hat{x} = x/d_1$ |
| a_i , cm | $\hat{a}_i = a_i/d_1$ |
| d_i , cm | $\hat{d}_i = d_i/d_1$ |
| t , s | $\hat{t} = tD_{S_1}/d_1^2$ |
| T_F , s | $\hat{T}_F = T_FD_{S_1}/d_1^2$ |
| S_i , M | $\hat{S}_i = S_i/K_M$ |
| P_i , M | $\hat{P}_i = P_i/K_M$ |
| C_{50} , M | $\hat{C}_{50} = C_{50}/K_M$ |
| D_{S_i} , cm ² /s | $\hat{D}_{S_i} = D_{S_i} / D_{S_1}$ |
| D_{P_i} , cm ² /s | $\hat{D}_{P_i} = D_{P_i} / D_{S_1}$ |
| I , A/cm ² | $\hat{I} = Id_1/(n_eFD_{P_1}K_M)$ |

follows ($\hat{t} > 0$):

$$\frac{\partial \hat{S}_1}{\partial \hat{t}} = \frac{\partial^2 \hat{S}_1}{\partial \hat{x}^2} - \alpha^2 \frac{\hat{S}_1}{1 + \hat{S}_1}, \quad (2.29a)$$

$$\frac{\partial \hat{P}_1}{\partial \hat{t}} = \hat{D}_{P_1} \frac{\partial^2 \hat{P}_1}{\partial \hat{x}^2} + \alpha^2 \frac{\hat{S}_1}{1 + \hat{S}_1}, \quad \hat{x} \in (0, 1), \quad (2.29b)$$

where α^2 is the diffusion module, also known as the Damköhler number [15],

$$\alpha^2 = \frac{d_1^2 V_{\max}}{D_{S_1} K_M}. \quad (2.30)$$

The diffusion module α^2 compares the rate of the enzyme reaction (V_{\max}/K_M) with the rate of the mass transport through the enzyme layer (D_{S_1}/d_1^2).

The diffusion equations (2.19) are transformed as follows ($\hat{t} > 0$):

$$\frac{\partial \hat{S}_i}{\partial \hat{t}} = \hat{D}_{S_i} \frac{\partial^2 \hat{S}_i}{\partial \hat{x}^2}, \quad (2.31a)$$

$$\frac{\partial \hat{P}_i}{\partial \hat{t}} = \hat{D}_{P_i} \frac{\partial^2 \hat{P}_i}{\partial \hat{x}^2}, \quad \hat{x} \in (\hat{a}_{i-1}, \hat{a}_i), \quad i = 2, 3, \quad (2.31b)$$

The initial conditions (2.20) take the following form ($i = 1, 2$):

$$\hat{S}_i(\hat{x}, 0) = 0, \quad \hat{P}_i(\hat{x}, 0) = 0, \quad \hat{x} \in [\hat{a}_{i-1}, \hat{a}_i], \quad (2.32a)$$

$$\hat{S}_3(\hat{x}, 0) = \begin{cases} 0, & \hat{x} \in [\hat{a}_2, \hat{a}_3), \\ \hat{S}_0, & \hat{x} = \hat{a}_3, \end{cases} \quad (2.32b)$$

$$\hat{P}_3(x, 0) = 0, \quad \hat{x} \in [\hat{a}_2, \hat{a}_3], \quad (2.32c)$$

The matching conditions (2.21) transform in to the following conditions ($\hat{t} > 0$, $i = 1, 2$):

$$\hat{D}_{S_i} \frac{\partial \hat{S}_i}{\partial \hat{x}} \Big|_{\hat{x}=\hat{a}_i} = \hat{D}_{S_{i+1}} \frac{\partial \hat{S}_{i+1}}{\partial \hat{x}} \Big|_{\hat{x}=\hat{a}_i}, \quad (2.33a)$$

$$\hat{S}_i(\hat{a}_i, \hat{t}) = \hat{S}_{i+1}(\hat{a}_i, \hat{t}), \quad (2.33b)$$

$$\hat{D}_{P_i} \frac{\partial \hat{P}_i}{\partial \hat{x}} \Big|_{\hat{x}=\hat{a}_i} = \hat{D}_{P_{i+1}} \frac{\partial \hat{P}_{i+1}}{\partial \hat{x}} \Big|_{\hat{x}=\hat{a}_i}, \quad (2.33c)$$

$$\hat{P}_i(\hat{a}_i, \hat{t}) = \hat{P}_{i+1}(\hat{a}_i, \hat{t}). \quad (2.33d)$$

The boundary conditions (2.22)-(2.24) take the following form ($\hat{t} > 0$):

$$\hat{P}_1(0, \hat{t}) = 0, \quad \frac{\partial \hat{S}_1}{\partial \hat{x}} \Big|_{\hat{x}=0} = 0, \quad (2.34a)$$

$$\hat{P}_3(\hat{a}_3, \hat{t}) = 0, \quad (2.34b)$$

$$\hat{S}_3(\hat{a}_3, \hat{t}) = \begin{cases} \hat{S}_0, & \hat{t} \leq \hat{T}_F, \\ 0, & \hat{t} > \hat{T}_F. \end{cases} \quad (2.34c)$$

The dimensionless current (flux) \hat{I} is defined as follows:

$$\hat{I}(\hat{t}) = \left. \frac{\partial \hat{P}_1}{\partial \hat{x}} \right|_{\hat{x}=0} = \frac{I(t)d_1}{n_e F D_{P_1} K_M}. \quad (2.35)$$

Assuming the same diffusion coefficients of the substrate and the product, the initial set of model parameters reduces to the following aggregate dimensionless parameters: \hat{d}_2 the thickness of the dialysis membrane, \hat{d}_3 the diffusion layer thickness, α^2 the diffusion module, \hat{T}_F the injection time, \hat{S}_0 the substrate concentration in the bulk during the injection, and $\hat{D}_{S_i} = D_{S_i}/D_{S_1} = D_{P_i}/D_{P_1} = \hat{D}_{P_i}$ - the ratio of the diffusion coefficient in the dialysis membrane (at $i = 2$) or in the diffusion layer (at $i = 3$) to the respective diffusion coefficient in the enzyme layer.

The diffusion module α^2 is one of the most important parameters that essentially define internal characteristics of layered amperometric biosensors [15, 35–37]. The biosensor response is known to be under diffusion control as $\alpha^2 \gg 1$. In the opposite case, where $\alpha^2 \ll 1$, the enzyme kinetics predominates in the response.

2.2.9 Numerical simulation

The mathematical model and the numerical solution were validated using the known analytical solution [15]. Assuming $T_F \rightarrow \infty$ and $d_2 \rightarrow 0$ or $d_3 \rightarrow 0$, the mathematical model (2.18)-(2.25) approaches the two-compartment model of the amperometric biosensor, acting in the batch mode [15]. The three compartment model approaches the two compartment model also in the unrealistic case, where the diffusion coefficients for the dialysis membrane are assumed to be the same as for the diffusion layer, $D_{S_2} = D_{S_3}$ and $D_{P_2} = D_{P_3}$. Additionally assuming $S_0 \ll K_M$, the nonlinear Michaelis-Menten reaction function in (2.18) simplifies to a linear function $V_{\max}S_1/K_M$. Under these assumptions the model (2.18)-(2.25)

has been solved analytically [15]. Under the steady-state conditions a relative difference between the numerical and analytical solutions was smaller than 1%.

To investigate the effect of the dialysis membrane on the biosensor response, a number of experiments were carried out, while the values of some parameters were kept constant [69, 73],

$$\begin{aligned} K_M &= 100\mu\text{M}, \quad D_{S_1} = D_{P_1} = 300\mu\text{m}^2/\text{s}, \\ D_{S_2} = D_{P_2} &= 0.3D_{S_1}, \quad D_{S_3} = D_{P_3} = 2D_{S_1}, \\ n_e &= 1, \quad d_1 = 200\mu\text{m}, \quad d_3 = 20\mu\text{m}. \end{aligned} \quad (2.36)$$

To minimize the effect of the Nernst diffusion layer on the biosensor response, the responses were simulated at a practically minimal thickness ($d_3 = 20\mu\text{m}$) of the external diffusion layer assuming, well stirred buffer solution by a magnetic stirrer [69].

Fig. 2.6 illustrates the evolution of the density $I(t)$ of the biosensor current simulated at a moderate concentration S_0 of the substrate ($S_0 = K_M$) and different values of the other model parameters: the maximal enzymatic rate V_{\max} (0.75 and $1.5\mu\text{M}$), the injection time T_F (3 and 6 s) and the thickness d_2 of the dialysis membrane (10 and $20\mu\text{m}$). Assuming (2.36), these two values of the maximal enzymatic rate V_{\max} correspond to the following two values of the dimensionless diffusion module α^2 : 1 and 2. Accordingly, $d_2 = 10\mu\text{m}$ corresponds to the dimensionless relative thickness \hat{d}_2 of the dialysis membrane equal to 0.05, while $d_2 = 20\mu\text{m}$ leads to $\hat{d}_2 = 0.1$.

Fig. 2.6 illustrates a non-monotonous behaviour of the biosensor current. In all the simulated cases, the current increases with the increasing time t up to the injection time T_F ($t \leq T_F$). However, the current also increases some time after the substrate disappears from the bulk solution ($t \geq T_F$). The time moment T_{\max} of the peak current and the peak current I_{\max} depends on the model parameters: V_{\max} , T_F and d_2 . In all the simulated cases, the time moment of the peak current

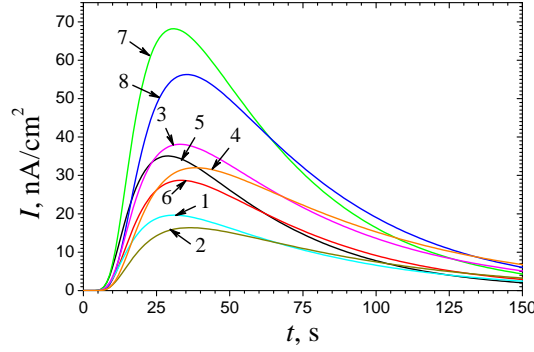


Figure 2.6: Dynamics of the Biosensor Response; V_{\max} : 0.75 (1-4), 1.5 μM (5-8), T_F : 3 (1, 2, 5, 6), 6 s (3, 4, 7, 8); d_2 : 10 (1, 3, 5, 7), 20 μm (2, 4, 6, 8)

was larger than T_F ($T_{\max} > T_F$).

In Fig. 2.6 we see, that different values of the model parameters V_{\max} and d_2 , the density I_{\max} of the maximal current increases almost two times when the injection time T_F doubles. However, the influence of doubling the time T_F on the time of the maximal current is rather slight. When comparing curves 1 ($T_F = 3$) and 3 ($T_F = 6$ s), one can see that the time T_{\max} of the maximal response increases from 31 only to 33 s, while I_{\max} increases from 19.7 up to 38 nA/cm^2 as $V_{\max} = 0.75 \mu\text{M}$ ($\alpha^2 = 2$) and $d_2 = 10 \mu\text{m}$ ($\hat{d}_2 = 0.1$).

Fig. 2.6 also shows that the biosensor response noticeably depends on the thickness d_2 of the dialysis membrane. An increase in d_2 prolongs the time of the maximal current. As one can see in Fig. 2.6 that the maximal current decreases when the thickness d_2 of the dialysis membrane increases. FIA biosensing systems have been already investigated by using mathematical models at zero thickness of the dialysis membrane [40, 56]. Fig. 2.6 visually substantiates the importance of the dialysis membrane.

2.2.10 Results and discussion

Using the numerical simulation, the biosensor action was analysed with a special emphasis on the conditions under which the biosensor sensitivity can be increased and the calibration curve can be prolonged by changing the biosensor geometry (especially the thickness of the dialysis membrane), the injection duration, and the catalytic activity of the enzyme. In order to investigate the influence of the model parameters on the half maximal effective concentration C_{50} of the substrate, the simulation was performed in a wide range of values of the thickness d_2 of the dialysis membrane, the diffusion module α^2 , and the injection time T_F .

The dimensionless half-maximal effective concentration \hat{C}_{50} expresses the relative prolongation (in times) of the calibration curve in comparison with the theoretical Michaelis constant K_M . For the biosensor of a concrete configuration, the concentration C_{50} as well as the half-maximal effective concentration constant can be quite easily calculated by a multiple simulation of the maximal response changing the substrate concentration S_0 [35, 56].

Fig. 2.7 shows the dependence of the dimensionless half-maximal effective concentration \hat{C}_{50} on the thickness d_2 of the dialysis membrane. The concentration C_{50} was calculated and then normalized with respect to the Michaelis constant K_M at three values of the diffusion module α^2 : 0.1 (curves 1 and 2), 1 (3, 4) and 10 (5, 6), and two practically extreme values of the injection time T_F : 1 (1, 3, 5) and 10 s (2, 4, 6). At all these values of α^2 and T_F , simulations have been performed by changing the thickness d_2 from $5\ \mu\text{m}$ ($\hat{d}_2 = 0.025$) to $40\ \mu\text{m}$ ($\hat{d}_2 = 0.2$).

One can see in Fig. 2.7, that the dimensionless half-maximal effective concentration \hat{C}_{50} (as well as the respective dimensional concentration C_{50}) is a monotonous by increasing function of the thickness d_2 of the dialysis membrane. An increase in the thickness d_2 noticeably prologs a linear part of the calibra-

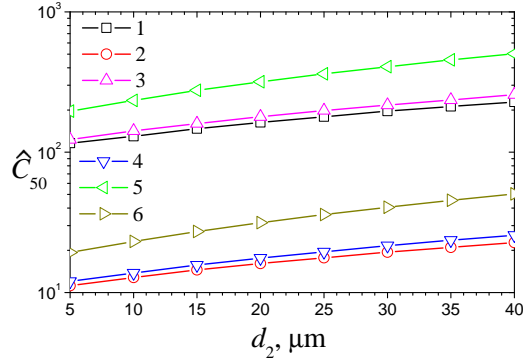


Figure 2.7: Effective Concentration \hat{C}_{50} vs. Thickness d_2 of the Dialysis Membrane; α^2 : 0.1 (1, 2), 1 (3, 4), 10 (5, 6), T_F : 1 (1, 3, 5), 10 s (2, 4, 6)

tion curve of the biosensor. It can be explained by increasing an additional external diffusion limitation, caused by increasing the thickness of the membrane [32, 33, 59, 64]. This figure also illustrates a significant dependence of C_{50} on the diffusion module α^2 , as $\alpha^2 \leq 1$.

To properly investigate the impact of the injection time T_F on the length of the linear part of the calibration curve, the dimensionless half-maximal effective concentration \hat{C}_{50} was also calculated by changing T_F from 0.5 up to 10 s. The values of \hat{C}_{50} were calculated by three values of the diffusion module α^2 (0.1, 1, and 10) and two values of the thickness d_2 (10 and 20 μm) of the dialysis membrane. The calculation results are presented in Fig. 2.8.

Fig. 2.8 shows that \hat{C}_{50} approximately exponentially increases with a decrease in the injection time T_F . The calibration curve of the biosensor can be prolonged by more than an order of magnitude only with a decrease in the injection time T_F . This impact of T_F on the biosensor sensitivity only slightly depends on the thickness d_2 of the dialysis membrane and the diffusion module α^2 . A similar effect was also noticed when modelling a more simple biosensor containing no dialysis membrane [56].

Fig. 2.8 also demonstrates that demonstrates the effective concentration \hat{C}_{50} is

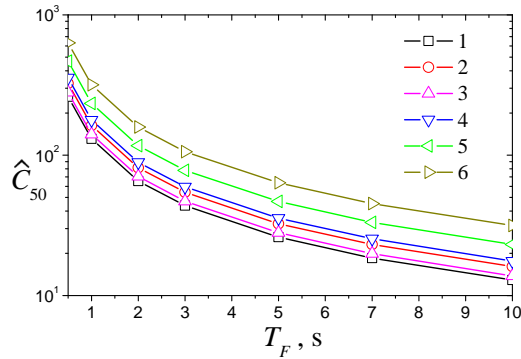


Figure 2.8: Effective Concentration \hat{C}_{50} vs. Injection Time T_F ; α^2 : 0.1 (1, 2), 1 (3, 4), 10 (5, 6), d_2 : 10 (1, 3, 5), 20 μm (2, 4, 6)

noticeably higher at greater values of the diffusion module α^2 than at lower ones.

To investigate the impact of the diffusion module α^2 on the effective concentration, biosensor responses were simulated in a wide range of values of α^2 . The simulation results are presented in Fig. 2.9. The effective concentration \hat{C}_{50} was calculated at two values of the thickness d_2 (10 and 20 μm) of the dialysis membrane and two values of the injection time T_F (1 and 10 s). At concrete values of d_2 and T_F , the calculations were performed by changing the maximal enzymatic rate V_{max} from 75 nM/s ($\alpha^2 = 0.1$) to 7.5 $\mu\text{M/s}$ ($\alpha^2 = 10$), while keeping all the other parameters constant.

As one can see in Fig. 2.9, the effective concentration \hat{C}_{50} is a monotonous increasing function of α^2 . When the enzyme kinetics predominates in the biosensor response ($\alpha^2 \ll 1$) the concentration \hat{C}_{50} almost constant function. In the opposite case of the biosensor operation, if the biosensor response is under diffusion control ($\alpha^2 \gg 1$), the concentration \hat{C}_{50} exponentially increases with an increase in the diffusion module α^2 . A similar influence of the diffusion module α^2 on the linear part of the calibration curve was also noticed when modelling the corresponding biosensor with no dialysis membrane [56].

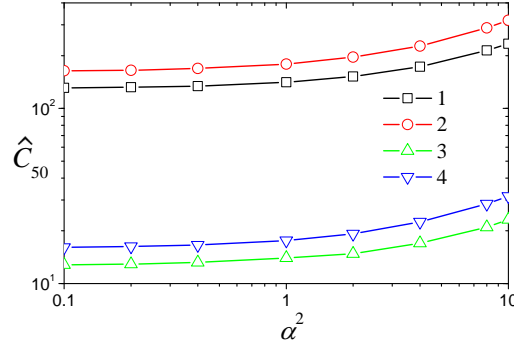


Figure 2.9: Effective Concentration \hat{C}_{50} vs. Diffusion Module α^2 ; d_2 : 10 (1, 3), $20 \mu\text{m}$ (2, 4), T_F : 1 (1, 2), 10 s (3, 4)

In real applications of biosensors, the diffusion module α^2 can be controlled by changing the maximal enzyme activity V_{\max} as well as the thickness d_1 of the enzyme layer. The maximal enzymatic rate V_{\max} is actually a product of two parameters: the catalytic constant k_2 , introduced in (1.1), and the total concentration of the enzyme [32, 33]. Since, in actual applications it is usually impossible to change a value of the constant k_2 , the maximal rate V_{\max} as well as the diffusion module α^2 might be changed by changing the enzyme concentration in the enzyme layer.

2.2.11 Section summary

The mathematical model (2.18)-(2.25) of an amperometric biosensor, containing a dialysis membrane and utilizing the flow injection analysis, can be successfully used to investigate the kinetic peculiarities of the biosensor response. The respective dimensionless mathematical model (2.29)-(2.35) can be applied in the numerical investigation of the impact of model parameters on the biosensor action and to optimize the biosensor configuration.

By increasing the thickness d_2 of the dialysis membrane, the half-maximal effective concentration \hat{C}_{50} can be increased and the linear part of the biosensor

calibration curve can be prolonged for several fold, see Fig. 2.7.

The half-maximal effective concentration \hat{C}_{50} approximately exponentially increases with a decrease in the injection time T_F . The calibration curve of the biosensor can be prolonged by a few orders of magnitude by decreasing the injection time T_F Fig. 2.8.

The half maximal effective concentration \hat{C}_{50} is a monotonous increasing function of the diffusion module α^2 . When the enzyme kinetics distinctly predominates in the response ($\alpha^2 \ll 1$), \hat{C}_{50} is approximately a constant function of α^2 , while as $\alpha^2 \gg 1$ the concentration \hat{C}_{50} exponentially increases with an increase in α^2 Fig. 2.9.

2.3 Computational modelling and validation of a multilayer amperometric biosensor

Recently, an innovative approach in design of biosensors, based on carbon nanotubes (CNT) layer deposited on the polycarbonate perforated membrane, has been proposed [74] and computationally modelled [56]. Then, the approach was expanded by replacing the CNT-based electrode with a simpler and cheaper carbon paste electrode, combining with an additional lavesan membrane. The aim of this work was to develop a mathematical model of an amperometric mediated biosensor, based on an enzyme layer and two supporting porous membranes. The proposed model is based on nonlinear non-stationary reaction-diffusion equations. The model was described in a one-dimensional-in-space domain and consists of four layers (compartments): a layer of enzyme solution entrapped into electrode, a polyvinyl alcohol (PVA) membrane, a lavesan membrane and an outer diffusion layer. The numerical simulation was performed under transient conditions, using the finite difference technique [15, 35, 41]. The mathematical

model and the numerical solution were validated by experimental data. The obtained agreement between the simulation results and the experimental data was admissible at different concentrations of the substrate to be analyzed.

2.3.1 Mathematical model

Fig. 2.10 shows a schematic representation of a biosensor to be modelled. The considered biosensor consists of several layers of different materials and sizes. An electrode and a relatively thin layer of an enzyme (an enzyme membrane, region L_1), applied onto the electrode surface, are the basic parts of the biosensor. The enzyme layer is covered by two permeable membranes: a polyvinyl alcohol (PVA) membrane (region L_2) and a lavesan membrane (L_3). In the enzyme layer, the enzymatic reaction as well as the mass transport by diffusion of the substrate, mediator and reaction product take place. Due to the immobilization no mass transport of the enzyme occurs. In two other membranes as well as in the diffusion limiting region only the mass transport by diffusion takes place. The model also involves a convective region (L_4) where the concentrations of all the species are maintained constant.

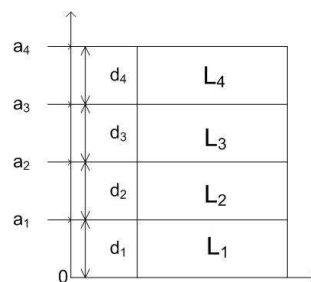
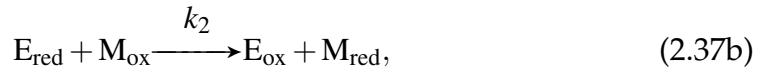


Figure 2.10: The principal structure of the modelled biosensor.

In the enzyme layer we consider a two-stage enzyme-catalyzed reaction



where the substrate (S) combines with an enzyme (E) to form a product (P) in the presence of the mediator (M) [56]. There E_{ox} stands for the oxidised enzyme, while E_{red} - for the reduced forms of the enzyme. Respectively, M_{ox} and M_{red} represent the oxidised and reduced forms of the mediator.

On the electrode surface the mediator is electrochemically re-oxidised and electrons are released creating the current as an output result,



As it is common for the amperometric biosensors, the electrochemical reaction (2.38) is assumed to be very fast [19, 33].

The substrate S to be analysed gets into the biosensor area from the buffer solution through the porous lavesan and PVA membrane. The external diffusion layer can be treated as the Nernst diffusion layer [41]. According to the Nernst approach the layer of the thickness d_4 remains unchanged with time. It is also assumed that away from it the solution is a uniform in the concentration.

2.3.2 Governing equations

Due to the symmetrical geometry of the electrode and a homogeneous distribution of the immobilized enzyme in the enzyme layer of a uniform thickness, the

mathematical model of the biosensor action can be defined in a one-dimensional-in-space domain [15, 16, 35]. Coupling the enzyme catalyzed reaction (2.37) in the enzyme layer with the mass transport by diffusion, described by Fick's law, leads to the following system of nonlinear reaction-diffusion equations:

$$\frac{\partial E_{ox}}{\partial t} = k_2 M_{ox,1} E_{red} - k_1 E_{ox} S_1, \quad (2.39a)$$

$$\frac{\partial E_{red}}{\partial t} = -k_2 M_{ox,1} E_{red} + k_1 E_{ox} S_1, \quad (2.39b)$$

$$\frac{\partial M_{ox,1}}{\partial t} = D_{M_{ox,1}} \Delta M_{ox,1} - k_2 M_{ox,1} E_{red,1}, \quad (2.39c)$$

$$\frac{\partial M_{red,1}}{\partial t} = D_{M_{red,1}} \Delta M_{red,1} + k_2 M_{ox,1} E_{red,1}, \quad (2.39d)$$

$$\frac{\partial S_1}{\partial t} = D_{S_1} \Delta S_1 - k_1 E_{ox,1} S_1, \quad x \in (0, a_1), \quad t > 0, \quad (2.39e)$$

where x and t denote for space and time, S_1 is the concentration of the substrate (S) in the enzyme layer, E_{ox} , E_{red} , $M_{ox,1}$ and $M_{red,1}$ stand for the molar concentrations of the oxidised and reduced forms of the enzyme and mediator, respectively, D_{S_1} , $D_{M_{ox,1}}$, $D_{M_{red,1}}$ are the constant diffusion coefficients, and $a_1 = d_1$ is the thickness of the enzyme layer [15, 36, 37]. The coefficients k_1 and k_2 are the rates of reactions (2.37a) and (2.37b), respectively. Since the product P has no influence on the biosensor response, the dynamics of the concentration P is not considered.

In the outer layer, only the mass transport by diffusion of both species takes place ($t > 0$),

$$\frac{\partial M_{ox,i}}{\partial t} = D_{M_{ox,i}} \Delta M_{ox,i}, \quad (2.40a)$$

$$\frac{\partial M_{red,i}}{\partial t} = D_{M_{red,i}} \Delta M_{red,i}, \quad (2.40b)$$

$$\frac{\partial S_i}{\partial t} = D_{S_i} \Delta S_i, \quad x \in (a_{i-1}, a_i), \quad i = 2, 3, 4, \quad (2.40c)$$

where S_i is the substrate concentration in the layer (a_{i-1}, a_i) , $M_{ox,i}$ and $M_{red,i}$ are

the concentrations of the oxidised and reduced forms of the mediator, respectively, $D_{S_1}, D_{M_{ox,1}}, D_{M_{red,1}}$ are constant diffusion coefficients, $i = 2, 3, 4$.

2.3.3 Initial and boundary conditions

Let $x = 0, x = a_1, x = a_2, x = a_3$, and $x = a_4$, respectively, represent the following boundaries: between the electrode and the enzyme layer, the enzyme layer and the PVA membrane, the PVA membrane and the lavesan membrane, the lavesan membrane and the external diffusion layer, the external diffusion layer and the bulk solution. The biosensor operation starts when the substrate and the mediator appear in the bulk solution ($t = 0$),

$$\begin{aligned} M_{ox,i}(x, 0) = 0, \quad M_{red,i}(x, 0) = 0, \\ S_i(x, 0) = 0, \quad x \in [a_{i-1}, a_i], \quad i = 2, 3, \end{aligned} \quad (2.41)$$

$$\begin{aligned} M_{ox,4}(x, 0) = 0, \quad M_{red,4}(x, 0) = 0, \\ S_4(x, 0) = 0, \quad x \in [a_3, a_4), \end{aligned} \quad (2.42)$$

$$\begin{aligned} M_{ox,4}(a_4, 0) = M_0, \quad M_{red,4}(a_4, 0) = 0, \\ S_4(a_4, 0) = S_0, \end{aligned} \quad (2.43)$$

$$E_{ox,0}(x, 0) = E_0, \quad E_{red,0}(x, 0) = 0, \quad x \in (0, a_1), \quad (2.44)$$

where S_0 and M_0 are concentrations of the substrate and the mediator in the buffer solution, and E_0 stands for the initial concentration of the enzyme.

Due to the electrode polarization, the concentration of the reduced mediator M_{red}

on the electrode surface ($x = 0$) is permanently reduced to zero ($t > 0$) [15, 35],

$$M_{red,1}(0,t) = 0. \quad (2.45)$$

The mediator re-oxidation reaction (2.38) is assumed to be so fast, that the whole diffusive mediator M_{red} , touching the electrode surface ($x = 0$), is immediately re-oxidised, i.e. M_{red} is converted to M_{ox} ($t > 0$),

$$D_{M_{red,1}} \frac{\partial M_{red,1}}{\partial x} \Big|_{x=0} = - D_{M_{ox,1}} \frac{\partial M_{ox,1}}{\partial x} \Big|_{x=0}. \quad (2.46)$$

The substrate concentration flux on the electrode surface equals zero because of the substrate electro-inactivity ($t > 0$),

$$\frac{\partial S_1}{\partial x} \Big|_{x=0} = 0. \quad (2.47)$$

The outer diffusion layer ($a_3 < x < a_4$) is treated as the Nernst diffusion layer [41]. According to the Nernst approach, the layer of the thickness $d_4 = a_4 - a_3$ remains unchanged with time, and away from it the solution is uniform in the concentration ($t > 0$),

$$\begin{aligned} M_{ox,4}(a_4,t) &= M_0, & M_{red,4}(a_4,t) &= 0, \\ S_4(a_4,t) &= S_0. \end{aligned} \quad (2.48)$$

The fluxes of the substrate and the mediator (in oxidised and reduced forms) through the stagnant external layer are assumed to be equal to the corresponding fluxes entering the surface of the enzyme membrane. Because of this, on the boundary between adjacent regions with different diffusivities, we define the

following matching conditions ($t > 0$, $i = 1, 2, 3$):

$$D_{S_i} \frac{\partial S_i}{\partial x} \Big|_{x=a_i} = D_{S_{i+1}} \frac{\partial S_{i+1}}{\partial x} \Big|_{x=a_i}, \quad (2.49)$$

$$S_i(a_i, t) = S_{i+1}(a_i, t),$$

$$D_{M_{ox,i}} \frac{\partial M_{ox,i}}{\partial x} \Big|_{x=a_i} = D_{M_{ox,i+1}} \frac{\partial M_{ox,i+1}}{\partial x} \Big|_{x=a_i}, \quad (2.50)$$

$$M_{ox,i}(a_i, t) = M_{ox,i+1}(a_i, t),$$

$$D_{M_{red,i}} \frac{\partial M_{red,i}}{\partial x} \Big|_{x=a_i} = D_{M_{red,i+1}} \frac{\partial M_{red,i+1}}{\partial x} \Big|_{x=a_i}, \quad (2.51)$$

$$M_{red,i}(a_i, t) = M_{red,i+1}(a_i, t).$$

2.3.4 Biosensor response

The anodic or cathodic current is measured as a result of a physical experiment. The current is proportional to the gradient of the mediator concentration on the electrode surface, i.e. on the border $x = 0$. The biosensor current $I(t)$ at time t can be obtained explicitly from Faraday's and Fick's laws [15],

$$I(t) = n_e F A D_{M_{red,1}} \frac{\partial M_{red,1}}{\partial x} \Big|_{x=0} \quad (2.52)$$

$$= -n_e F A D_{M_{ox,1}} \frac{\partial M_{ox,1}}{\partial x} \Big|_{x=0}, \quad (2.53)$$

where n_e is the number of electrons involved in charge transfer, A is the area of the electrode surface, and F is the Faraday constant.

We assume that system (2.39)–(2.51) achieves an equilibrium as $t \rightarrow \infty$,

$$I_\infty = \lim_{t \rightarrow \infty} I(t). \quad (2.54)$$

where I_∞ is the steady-state biosensor current. The steady-state current is the main characteristic in commercial amperometric biosensors, acting in the batch mode [19, 32, 33].

2.3.5 Dimensionless model

In order to extract the main governing parameters of the mathematical model, thus reducing the number of model parameters in general, a dimensionless model is often derived [15, 61, 67]. Replacement of the parameters is based on parameter mappings eliminating model dimensional parameters. The following table presents all the dimensionless parameters of the model:

Table 2.3: Model parameters

| Dimensional | Dimensionless |
|---|--|
| $x, \text{ cm}$ | $\hat{x} = x/d_1$ |
| $t, \text{ s}$ | $\hat{t} = tD_{M_{ox,1}}/d_1^2$ |
| $E_{ox}, \text{ M}$ | $\hat{E}_{ox} = E_{ox}/E_0$ |
| $E_{red}, \text{ M}$ | $\hat{E}_{red} = E_{red}/E_0$ |
| $S_i, \text{ M}$ | $\hat{S}_i = S_i/S_0$ |
| $M_{ox,i}, \text{ M}$ | $\hat{M}_{ox,i} = M_{ox,i}/M_0$ |
| $M_{red,i}, \text{ M}$ | $\hat{M}_{red,i} = M_{red,i}/M_0$ |
| $D_{M_{ox,i}}, \text{ cm}^2/\text{ s}$ | $\hat{D}_{M_{ox,i}} = D_{M_{ox,i}} / D_{M_{ox,1}}$ |
| $D_{M_{red,i}}, \text{ cm}^2/\text{ s}$ | $\hat{D}_{M_{red,i}} = D_{M_{red,i}} / D_{M_{ox,1}}$ |
| $D_{S_i}, \text{ cm}^2/\text{ s}$ | $\hat{D}_{S_i} = D_{S_i} / D_{M_{ox,1}}$ |
| $I, \text{ A}$ | $\hat{I} = Id_1/(n_eFAD_{M_{red,1}}M_0)$ |

For the enzyme layer, reaction-diffusion equations (2.39) can be rewritten in the

following dimensionless form ($\hat{t} > 0, \hat{x} \in (0, 1)$):

$$\frac{\partial \hat{E}_{ox}}{\partial \hat{t}} = \alpha_2 \hat{M}_{ox,1} \hat{E}_{red} - \alpha_1 \hat{E}_{ox} \hat{S}_1, \quad (2.55a)$$

$$\frac{\partial \hat{E}_{red}}{\partial \hat{t}} = -\alpha_2 \hat{M}_{ox,1} \hat{E}_{red} + \alpha_1 \hat{E}_{ox} \hat{S}_1, \quad (2.55b)$$

$$\frac{\partial \hat{M}_{ox,1}}{\partial \hat{t}} = \hat{D}_{M_{ox,1}} \frac{\partial^2 \hat{M}_{ox,1}}{\partial \hat{x}^2} - \alpha_2 \hat{M}_{ox,1} \hat{E}_{red,1}, \quad (2.55c)$$

$$\frac{\partial \hat{M}_{red,1}}{\partial \hat{t}} = \hat{D}_{M_{red,1}} \frac{\partial^2 \hat{M}_{red,1}}{\partial \hat{x}^2} + \alpha_2 \hat{M}_{ox,1} \hat{E}_{red,1}, \quad (2.55d)$$

where all the unknown and model parameters are dimensionless. α_1 and α_2 are diffusion modules, also known as Damköhler numbers [15],

$$\alpha_1 = \frac{k_1 E_0 d_1^2}{D_{M_{ox,1}}}, \quad (2.56a)$$

$$\alpha_2 = \frac{k_2 E_0 d_1^2}{D_{M_{ox,1}}}. \quad (2.56b)$$

The diffusion module α_j compares the rate of the enzyme reaction $k_j E_0$ with the diffusion rate $D_{M_{ox,1}}/d_1^2$, $j = 1, 2$. It is rather well known that an ordinary enzyme electrode acts under diffusion limitation when the diffusion modulus is much higher than a unity [15, 36]. If the diffusion modulus is significantly smaller than a unity then the enzyme kinetics predominates in the biosensor response.

Governing equations (2.40) are transformed into the following dimensionless form ($\hat{t} > 0, \hat{x} \in (a_{i-1}/d_1, a_i/d_1)$):

$$\frac{\partial \hat{M}_{ox,i}}{\partial \hat{t}} = \hat{D}_{M_{ox,i}} \frac{\partial^2 \hat{M}_{ox,i}}{\partial \hat{x}^2}, \quad (2.57a)$$

$$\frac{\partial \hat{M}_{red,i}}{\partial \hat{t}} = \hat{D}_{M_{red,i}} \frac{\partial^2 \hat{M}_{red,i}}{\partial \hat{x}^2}, \quad (2.57b)$$

$$\frac{\partial \hat{S}_i}{\partial \hat{t}} = \hat{D}_{S_i} \frac{\partial^2 \hat{S}_i}{\partial \hat{x}^2}, \quad i = 2, 3, 4. \quad (2.57c)$$

The initial and boundary conditions can be transformed to a dimensionless form easily.

2.3.6 Numerical simulation

Some practical experiments were done to produce biosensor data. Different mediator values: $M_0^{(1)} = 200 \mu\text{M}$, $M_0^{(2)} = 50 \mu\text{M}$, $M_0^{(3)} = 5 \mu\text{M}$, the following parameters from physical experiments were given:

$$S_0^{(1)} = 0.49 \text{ mM}, \quad S_0^{(2)} = 0.99 \text{ mM}, \quad (2.58\text{a})$$

$$S_0^{(3)} = 1.99 \text{ mM}, \quad S_0^{(4)} = 4.98 \text{ mM}, \quad (2.58\text{b})$$

$$S_0^{(5)} = 9.9 \text{ mM}, \quad S_0^{(6)} = 19.6 \text{ mM} \quad (2.58\text{c})$$

The initial boundary value problem (2.39)–(2.51) was solved numerically because of nonlinearity of governing equations (2.39) [15, 35, 41]. In solving the biosensor model, an explicit finite difference scheme was developed applying a uniform discrete grid. Due to the biosensor geometry and after carrying out a number of experiments, some of the parameters were fixed and kept constant [56, 74]:

$$\begin{aligned} D_{M_{ox,1}} &= D_{M_{ox,1}} = D_{S_1} = 3 \mu\text{m}^2/\text{s}, \\ D_{M_{ox,2}} &= D_{M_{ox,2}} = D_{S_2} = 4.2 \mu\text{m}^2/\text{s}, \\ D_{M_{ox,3}} &= D_{M_{ox,3}} = D_{S_3} = 3.75 \mu\text{m}^2/\text{s}, \\ D_{M_{ox,4}} &= D_{M_{ox,4}} = D_{S_4} = 6 \mu\text{m}^2/\text{s}, \\ k_1 &= 6.9 \times 10^8 \text{ s}^{-1}, \quad k_2 = 4 \times 10^{10} \text{ s}^{-1}, \\ d_1 &= d_2 = 0.2 \text{ mm}, \quad d_3 = 1 \text{ mm}, \quad d_4 = 15 \text{ mm}, \\ n_e &= 2, \quad A = 0.03 \text{ cm}^2, \quad E_0 = 12 \mu\text{M}. \end{aligned} \quad (2.59)$$

The precise determination of values of some model parameters was impossible [74]. Due to that, the values of those parameters were determined by multiple simulation of the biosensor response by fitting the simulation results to experimental data.

2.3.7 Results and discussion

The physical experiments were carried out more than 100 seconds, while the computer simulation was performed until a desired accuracy of the steadystate current has been achieved, keeping the values of the model parameters, defined in (2.59), taking different mediator and substrate values. Fig. 2.11 shows the evolution of the biosensor current I , obtained experimentally (2, 4, 6, 8, 10 and 12) and numerically (1, 3, 5, 7, 9 and 11), the mediator concentration $M_0 = 200 \mu\text{M}$, and six concentrations of the substrate S_0 .

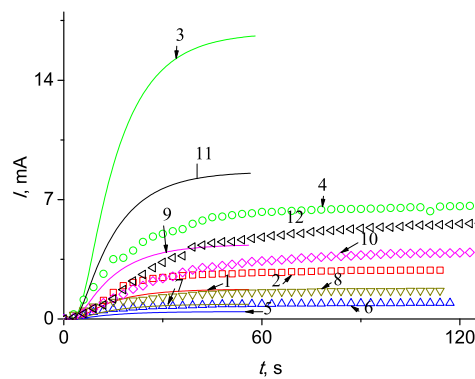


Figure 2.11: The dynamics of the biosensor current I obtained experimentally (2, 4, 6, 8, 10 and 12) and numerically (1, 3, 5, 7, 9 and 11) at $M_0^{(1)} = 200 \mu\text{M}$ and six concentrations of the substrate S_0 : 0.49 mM (5, 6), 0.99 mM (7, 8), 1.99 mM (1, 2), 4.98 mM (9, 10), 9.9 mM (11, 12), 19.6 mM (3, 4)

As one can see the obtained agreement between the simulation results and the experimental data is admissible at relatively low concentrations of the substrate,

i.e. the computational model matches the physical experiments. The simulated current tends to be stronger as compared to physical results when the concentration S_0 is larger than 4.98 mM. The same trend is seen in Fig. 2.12, where current I obtained experimentally (curves 2, 4, 6, 7, 9 and 11) and numerically (curves 1, 3, 5, 8, 10 and 12) at the value of the mediator concentration $M_0 = 50 \mu\text{M}$.

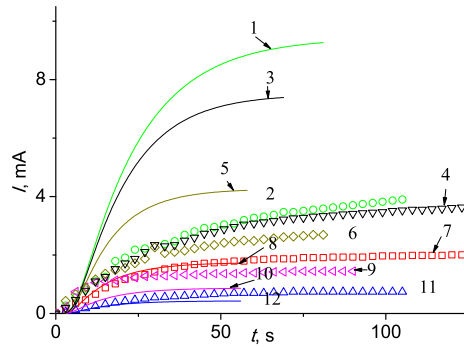


Figure 2.12: The dynamics of the biosensor current I obtained experimentally (2, 4, 6, 7, 9 and 11) and numerically (1, 3, 5, 8, 10 and 12) at $M_0^{(2)} = 50 \mu\text{M}$ and six concentrations of the substrate S_0 : 0.49 mM (11, 12), 0.99 mM (9, 10), 1.99 mM (7, 8), 4.98 mM (5, 6), 9.9 mM (3, 4), 19.6 mM (1, 2)

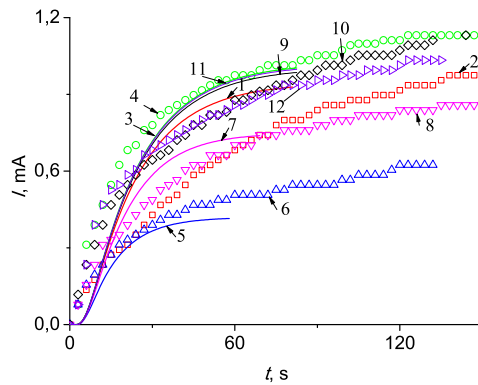


Figure 2.13: The dynamics of the biosensor current I obtained experimentally (2, 4, 6, 8, 10 and 12) and numerically (1, 3, 5, 7, 9 and 11) at $M_0^{(3)} = 5 \mu\text{M}$ and six concentrations of the substrate S_0 : 0.49 mM (5, 6), 0.99 mM (7, 8), 1.99 mM (1, 2), 4.98 mM (9, 10), 9.9 mM (11, 12), 19.6 mM (3, 4)

Fig. 2.13 illustrates further results taking even a lower concentration of the mediator $M_0^{(3)} = 5 \mu\text{M}$ and six concentrations of the substrate S_0 , including the practical results (2, 4, 6, 8, 10 and 12) and the results that obtained by computer model simulations (1, 3, 5, 7, 9 and 11).

As stated before, the results tend to differ more at greater concentrations of substance. Here we can see that at a lower $M_0^{(3)}$ value, the computer model yields closer results to the experimental ones at both lower and higher concentrations as compared to the values noticed in the previous results, seen in Fig. 2.11 and Fig. 2.12. To get indication about the variability of the obtained results, a relative error was calculated. In Fig. 2.14 and Fig. 2.15, the relative error of the calculations at $M_0^{(i)}$, $i = 1, 2, 3$ is presented (note that fracture in Fig. 2.14b is due to the absence of experimental data).

In Fig. 2.12 $S_0 = 1.99 \text{ mM}$ (curves 7 and 8), the relative error in Fig. 2.14b decreases from about 0.3 as $t = 10 \text{ s}$ to approximately 0 as $t = 42 \text{ s}$, while with larger values of t the error slightly increases. As $S_0 = 0.99 \text{ mM}$ (Fig. 2.12 curves 9 and 10), the relative error monotonously decreases from 1 at the initial stage of the biosensor operation to 0.4, while as $S_0 = 0.49 \text{ mM}$ (Fig. 2.12 curves 11 and 12), the relative error slightly increases from 0.25 to 0.4 both match at the final one ($t = 55 \text{ s}$).

In Fig. 2.15 we can see that as $S_0 = 1.99 \text{ mM}$, the relative error significantly increases from 0 as $t = 11 \text{ s}$ to 0.7 at $t = 20 \text{ s}$ and monotonously decreases to 0.25 as $t = 70 \text{ s}$. The curve of the relative error of other concentration curves decreases as $S_0 = 9.9 \text{ mM}$, $S_0 = 4.98 \text{ mM}$, $S_0 = 0.99 \text{ mM}$, $S_0 = 0.49 \text{ mM}$ (curves 2, 3, 5, 6, respectively), decreases to 0.2 - 0 and increase to 0.3 as $t = 45 \text{ s}$. At the higher concentration $S_0 = 19.6 \text{ mM}$, curve 1 monotonously decreases from $t = 3 \text{ s}$ to $t = 45 \text{ s}$

Rather large values of the relative error of the simulated responses indicate that the physical experiments are really more complex than that defined by the

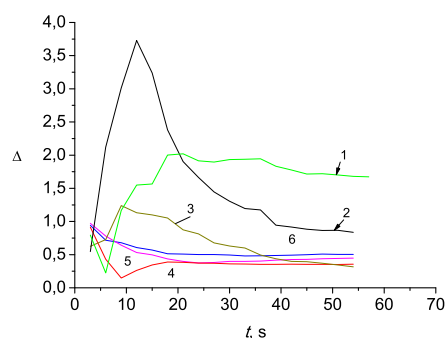
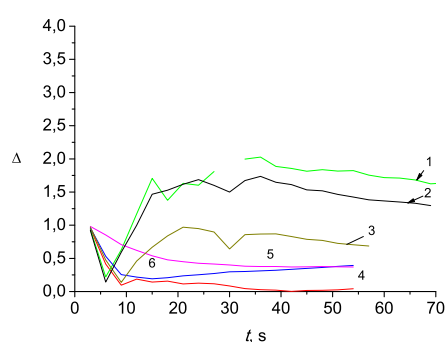
(a) $M_0^{(1)} = 200 \mu\text{M}$ (b) $M_0^{(2)} = 50 \mu\text{M}$

Figure 2.14: The change of the relative error of computer modelling compared to experimental data at specified $M_0^{(i)}$, $i = 1, 2$ values and six concentrations of the substrate S_0 : 0.49 mM (6), 0.99 mM (5), 1.99 mM (4), 4.98 mM (3), 9.9 mM (2), 19.6 mM (1)

mathematical model. Despite this inadequacy with the experiments, the model seems to be suitable for investigating the kinetic peculiarities and optimizing the configuration of the multilayer amperometric biosensor.

2.3.8 Section summary

Modelling of such a biosensor is complicated since we have to fit many parameters and to obtain an admissible agreement between the simulation results and the experimental data. In this work, only six validation curves were used,

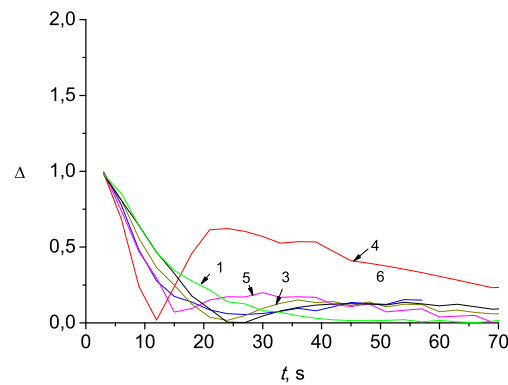


Figure 2.15: The change of the relative error of computer modelling compared to experimental data at $M_0^{(3)} = 5 \mu\text{M}$ and six concentrations of the substrate S_0 : 0.49 mM (6), 0.99 mM (5), 1.99 mM (4), 4.98 mM (3), 9.9 mM (2), 19.6 mM (1)

but this number of physical experiments was enough to conclude that model was not quite suitable for match experimental data in a wide range of substrate concentrations. On the other hand, on the basis of the given relative error analysis, the model was quite accurate at relatively low concentrations of the substrate. It must be taken into consideration that experimental data can also be inaccurate because of the external environment impact. The selected accuracy of the steady-state current did not have a perceptible effect on the simulation results.

Chapter 3

Quantitative analysis of mixtures

3.1 Optimization-Based Evaluation of Concentrations in modelling the Biosensor-Aided Measurement

We are interested in the establishment of the quantitative structure of a mixture, using observations of its properties and the known properties of its components. The problem is related to the measurement of concentrations of several known substrates in a solution, and can also be formulated as a problem of the evaluation of indirectly observable parameters; see e.g. [60, 75].

We assume that the structure of the function $z(t, x)$ is known: $z(t, x) = \sum_{j=1}^k y_j(t, x_j)$, $0 \leq t \leq t_{\max}$, $x = (x_1, \dots, x_k) \in X$ where functions $y_j(t, x_j)$ are supposed to be given. The parameter vector x should be evaluated using the observed values $w_i = z(t_i, x)$, $0 \leq t_i \leq t_{\max}$, $i = 1, \dots, n$. A large variety of subproblems of the general problem stated can be specified, and different methods can be appropriate for the solution of concrete subproblems. We focus on the problem related to the evaluation of concentrations of k substrates (components) in a mixture using a recorded signal of the biosensor w_i , $i = 1, \dots, n$, and records of similar signals of

the biosensor $y_j(t, x_j)$ applied to the liquid that contains only a single known substrate.

3.1.1 Mathematical model

The amperometric biosensor is an electrode with a relatively thin layer of enzymes (multi-enzyme membrane) applied onto the electrode surface. The enzyme-catalyzed reaction occurs in the enzyme layer of a biosensor. We consider a mixture of substrates (components) participating in the biochemical reaction network



where the substrate (S_j , combines with the enzyme (E_j) to issue the product (P_j), $j = 1, \dots, k$), [32, 33]. The rate of growth of the amount of the product is called the rate of reaction. No interaction between separate enzyme reactions is considered. Reactions in the biosensor are described by Flick's law which leads to the following equations:

$$\begin{aligned} \frac{\partial s_j}{\partial t} &= D_{S_j} \frac{\partial^2 s_j}{\partial \tau^2} - \frac{V_j s_j}{K_j + s_j}, \\ \frac{\partial p_j}{\partial t} &= D_{P_j} \frac{\partial^2 p_j}{\partial \tau^2} + \frac{V_j s_j}{K_j + s_j}, \\ 0 < \tau < d, \quad 0 < t \leq t_{\max}, \quad j &= 1, \dots, k, \end{aligned} \quad (3.2)$$

where $s_j(\tau, t)$ and $p_j(\tau, t)$ are the substrate and product concentrations in the enzyme layer, D_{S_j} , D_{P_j} are substrate and product diffusion coefficients, respectively, V_j is the maximal enzymatic rate attainable with that amount of enzyme, completely saturated with the substrate S_j , $j = 1, \dots, k$. K_j ($j = 1, \dots, k$) is the Michaelis constant, t is time, t_{\max} is the duration of the time interval in which the biosensor is analyzed, d is the thickness of the enzyme layer. During the substrates interaction with the biosensor the mass transport by diffusion takes

place, and the biochemical reactions start when the substrates appear on the enzyme layer because of the diffusion. Initial conditions ($t=0$) in the biosensor model are defined as follows:

$$s_j(\tau, 0) = \begin{cases} 0, & 0 \leq \tau < d, \\ S_o \cdot x_j, & \tau = d, \end{cases}$$

$$p_j(\tau, 0) = 0, \quad 0 \leq \tau \leq d, \quad j = 1, \dots, k, \quad (3.3)$$

where $S_o \cdot x_j$ is the concentration of substrate S_j , $S_o = 10^{-8} \text{ mol/cm}^3$. During the experiment the diffusion layer is constantly contiguous to the substrate solution; this fact in the batch mode is expressed by the following boundary conditions ($0 < t \leq t_{\max}$):

$$\left. \frac{\partial s_j}{\partial \tau} \right|_{\tau=0} = 0, \quad (3.4)$$

$$s_j(d, t) = S_o \cdot x_j, \quad t \leq t_{\max}, \quad (3.5)$$

$$p_j(0, t) = p_j(d, t) = 0, \quad j = 1, \dots, k. \quad (3.6)$$

In the injection mode the substrate appears in the bulk solutions only for short period of time, known as injection time (T_F). Later the substrate concentration is set to zero. Boundary conditions in the injection mode are defined as follows:

$$\left. \frac{\partial s_j}{\partial \tau} \right|_{\tau=0} = 0, \quad (3.7)$$

$$s_j(d, t) = \begin{cases} S_o \cdot x_j, & t \leq T_F \\ 0, & t > T_F \end{cases}, \quad (3.8)$$

$$p_j(0, t) = p_j(d, t) = 0, \quad j = 1, \dots, k. \quad (3.9)$$

3.1.2 Biosensor response

The current, measured as a result of a physical experiment, is proportional to the gradient of the reaction product concentration at the electrode surface, i.e. on the border $x = 0$. The density $y_j(t, x_j)$ of the biosensor current at time t can be obtained explicitly by Faraday's and Fick's laws [15],

$$y_j(t, x_j) = n_e F D p_j \left. \frac{\partial p_j}{\partial \tau} \right|_{\tau=0}, \quad j = 1, \dots, k, \quad (3.10)$$

where n_e is the number of electrons involved in the charge transfer, and F is the Faraday constant.

We assume that the system achieves the equilibrium as $t \rightarrow \infty$. The steady-state current is the main characteristic in commercial amperometric biosensors, acting in the batch mode [19, 32, 33]. The entire biosensor response $z(t, x)$ is the sum of individual biosensor currents $y_j(t, x_j), j = 1, \dots, k$.

3.1.3 Generated data

The computer software was developed to generate the biosensor response data in the batch and injection mode as well. In this work, the mathematical model, described above, was used to model real-world processes corresponding to the following parameters: $10^{-10} \text{ mol}/(\text{cm}^3\text{s}) \leq V_j \leq 10^{-7} \text{ mol}/(\text{cm}^3\text{s})$, $K_j = 10^{-7} \text{ mol}/\text{cm}^3$, $0 \leq t \leq 300 \text{ s}$, $0.01\text{cm} \leq d \leq 0.03\text{cm}$, and $0 \leq S_o \cdot x_j \leq 64 \cdot 10^{-8} \text{ mol}/\text{cm}^3$, $j = 1, \dots, k$, $k = 4$. The data for modelling are chosen the same as in [60, 75] where further details can be found.

The mixture consists of different compounds, each of which is characterized by its enzymatic rate V_j :

$$V_j = 10^{-6-k} \text{mol/cm}^3 \text{s}, \quad j = 1, \dots, k, k = 4 \quad (3.11)$$

The composition of each analysed mixture consists of different compounds. A variety of mixtures was obtained using the following values of $S_0^{(k)}$:

$$0 \leq S_0 \cdot x_j \leq 64 \cdot 10^{-8} \text{mol/cm}^3, j = 1, \dots, k, k = 4 \quad (3.12)$$

$$S_0 = 10^{-8} \text{mol/cm}^3, \quad (3.13)$$

$$1 \leq \alpha_m \leq 64. \quad (3.14)$$

Since as the amperometric biosensor simulations were carried out in two different modes, we chose the time when substrate contacts biosensors as follows: in the batch mode $T = 300\text{s}$ and in the injection mode $T_F = 10\text{s}$.

Using the parameters defined, in 3.12, simulations were performed only by changing the values of parameters V_j , $S_0 \cdot x_j$ and selecting the values of T and T_F according to the selected biosensor reaction mode.

$$I_{\vec{m}}^*(t_j) = \sum_{k=1}^K I_{m_k}^{(k)}(t_j), \quad \vec{m} = (m_1, \dots, m_K) \quad m_k = 1, \dots, m, \quad j = 1, \dots, N \quad (3.15)$$

$$(3.16)$$

It is supposed that a mixture contains up to 4 analytes, characterized by the reaction rate V_j . The output of the biosensor (current) y_j is recorded at the time moments $t_j = j$, $j = 1, \dots, T$. The output of the model also depends on

the biosensor parameter d , which is measured in centimeters, and denotes the thickness of the membrane.

3.1.4 Analysis of the available data

Biosensors are successfully applied to measure the concentration of a single known substrate in the presented liquid. The signal of the biosensor is measured in the steady state (i.e. for large enough t) for different specified concentrations, and the signal values are calibrated in the units of concentration. A linear dependency between the concentration and the value of the signal is desirable, and for many important applications biosensors with linear characteristics are available. When the presented liquid contains a mixture of substrates, the concentration measurement problem is more complicated, since the linearity of that characteristic for all the considered substrates in the range of concentrations of interest is normally difficult (or even impossible) to achieve. The same value of the signal in the steady state can be observed for different concentrations of substrates. Therefore the measurement of the signal value at the steady state only is not sufficient to establish concentrations for a mixture of components. We intend here to extract the information on concentrations from the observations over the transition process of a signal, i.e. during the time interval which starts from the moment when the biosensor contacts with the liquid of interest, and finishes at the steady state.

Let $w_i, i = 1, \dots, n$, be a sequence of recorded values of the biosensor signal at discrete time moments; technically the electric current, defined by (3.10), is recorded. Using the software implementation of the mathematical model of reactions in the biosensor, the signal $z(t, x)$ can be modelled in the form of a time $t \in T$ function, and of concentrations $x = (x_1, \dots, x_k)$, where T is the set of time moments t_i when the biosensor signal was recorded. If the measurements were

precise, the model would be ideally adequate, and the substrate concentrations in the model were the same as in the experiment, then w_i and $z(t_i, x)$ would be coincident. A natural idea is to evaluate unknown concentrations by fitting w_i with $z(t_i, x)$, $t_i \in T$, i.e. to accept the minimizer in the following problem as an estimate

$$\tilde{x} = \arg \min_{x \in X} f(W, Z(x)), \quad (3.17)$$

where $f(\cdot)$ denotes a measure of difference between $W = (w_1, \dots, w_n)$ and $Z(x) = (z(t_1, x), \dots, z(t_n, x))$. The following expression could be considered, for example, as a possible measure of difference

$$f_2(W, Z(x)) = \sum_{i=1}^n (w_i - z(t_i, x))^2. \quad (3.18)$$

The structure of minimization problem (3.17) corresponds to that of problems of nonlinear regression [76]. However, the formulated minimization problem is difficult to analyze, since the analytical properties of $z(t, x)$ are not known; moreover, computation of $z(t, x)$ is time consuming. The most serious difficulty here may be caused by the multimodality of the objective function. Another potential challenge is non-differentiability of $z(\cdot, x)$. In the least favourable case, where the functions $z(t, x)$ can coalesce for some different x , any method (not only optimization-based) for evaluating concentrations, using information on $z(t, x)$, would be challenged by the multiplicity of solutions. The problem should be considered as ill-defined if, for considerably different $x^{(1)}, x^{(2)}$, ($\|x^{(1)} - x^{(2)}\| > \Delta$), $z(\cdot, x^{(1)})$ and $z(\cdot, x^{(2)})$ would either coincide or differ but insignificantly. Due to these properties, (3.17) is a difficult global optimization problem [77]. For the general discussion on global optimization we refer to [78], and for the global optimization methods in nonlinear regression we refer to [79–81].

To state the considered practical problem in the form of an optimization problem that was numerically tractable, the establishment of favourable properties of the

objective function is crucial. Because of difficulties in the application of analytical methods to analyze the solutions of (3.2-3.10), in the present paper, the properties of $z(t, x)$ are investigated experimentally, using software implementation of the mathematical model developed in [35]. The measurements of the biosensor signal are replaced by those modelled. The errors of measurements are not taken into account, and computations are assumed ideally precise. The investigation of the influence of measurement errors and of the precision of computations would follow, if the results, obtained in the idealized case, were promising. By the replacement of experimental data by that generated according to the mathematical model, we somewhat ignore the complexities of the original real-world problem. But that seems inevitable, since such a replacement enables us to generate large amounts of data with desirable characteristics which would be impossible to collect experimentally because of the expensiveness and duration of experiments.

3.2 Analysis of the properties of the mathematical model

Let us start from a graphical illustration of signals of the biosensor modelled in both measurement modes: batch and injection; we refer to [60, 75] for details. The graphs of the biosensor signals in both modes are presented in Fig. 3.1 for four substrates with the parameter V_j equal to 10^{-6-j} , $j = 1, \dots, 4$, $d = 0.02\text{cm}$, and of the maximum concentration ($x_j = 64$).

From the left graphs in Fig. 3.1 it is obvious that the evaluation of concentrations in the batch mode is difficult (no matter which method would be used) because of two reasons at least: the scale similarity between the signals (especially corresponding to $V_1 = 10^{-7}$ and $V_2 = 10^{-8}$), and relatively small values of the

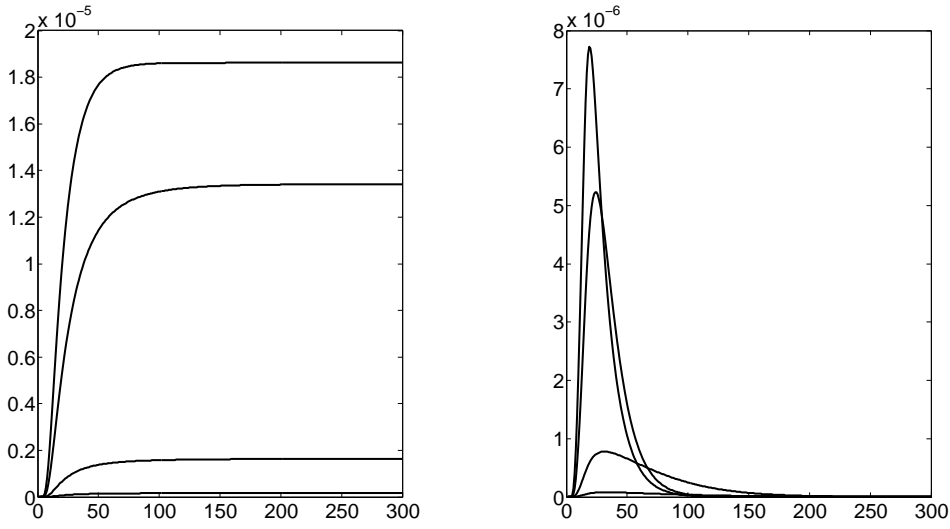


Figure 3.1: Signals of the biosensor in the batch mode on the left, and in the injection mode on the right. Each curve represents a measurement for a single substrate with $V_j = 10^{-6-j}$, and $x_j = 64$, $j = 1, \dots, 4$.

biosensor signal corresponding to $V_4 = 10^{-10}$ (the ratio of the signal values corresponding to $V_1 = 10^{-10}$ and $V_1 = 10^{-7}$ at $t = 300$ is equal to $8.8934 \cdot 10^{-4}$). The latter difficulty, caused by the potentially negligible influence of the fourth substrate, can also challenge the evaluation of concentration in the injection mode. However, the scale similarity in this case is not so evident.

The considered problem has been tackled in [60, 75] by approximating the straightforward mapping

$$\Phi: (w_1, \dots, w_n) \rightarrow x. \quad (3.19)$$

The approximation of $\Phi(\cdot)$ was constructed as the inverse of the mapping $x \rightarrow (w_1, \dots, w_n)$. The latter was defined according to (3.2-3.10) for $x \in C$ where C was a four-dimensional cubic mesh based on the following set of values of the components of x : $C = \{1, 2, 4, 8, 12, 16, 32, 64\}$. The set of 4096 biosensor signals

was considered, where the signals were modelled for the mixtures of four substrates with the concentrations defined by $x_j \in C$. Let us analyze the batch mode signals. If it were known a priori that $x_j \in C$, and were possible to measure the values of the signal $w_i = z(t_i, x)$ precisely, then x could be traced from the observation of a single value w_{300} . Such a conclusion is implied by the fact that the difference between the values w_{300} , corresponding to different x , is no less than $2.1 \cdot 10^{-13}$. However, to distinguish between these values, a super-precise equipment is needed with the measurement error no larger than $6.8 \cdot 10^{-6}\%$. In the case of measurement precision 0.1%, there are 374 indistinguishable pairs of signals, i.e. there exist 374 pairs $x^{(m)} \in C^4, x^{(r)} \in C^4$ such that

$$\max_{i=1, \dots, 300} \frac{|z(t_i, x^{(m)}) - z(t_i, x^{(r)})|}{\min\{z(t_{300}, x^{(m)}), z(t_{300}, x^{(r)})\}} < 0.001. \quad (3.20)$$

For example, two graphs of the signals, corresponding to the concentration vectors $x = (2, 64, 16, 32)$ and $x = (1, 64, 32, 12)$, practically coalesce; see the left graph of Fig. 3.2. However, if the signals are modelled for the same concentrations in the injection mode, they are still distinguishable, as seen from the right graph of Fig. 3.2.

The set of 4096 biosensor signals in [60, 75] was randomly bisected, and one part was used to train an artificial neural network that was used as an approximant of (3.19). The second part was used as an examination set. Several experiments have been done with different model parameters, corresponding to the various conditions of measurement, and some conclusions have been drawn about the precision of evaluations of x for the data related to $x \in C^4$. A qualitative conclusion in [60, 75] can be briefly formulated as follows: concentrations can be evaluated more precisely in the injection mode than in the batch mode, and the precision increases with an increase d . The quantitative estimates obtained for the data corresponding to C^4 , which is rather a rough discretization of X , are not

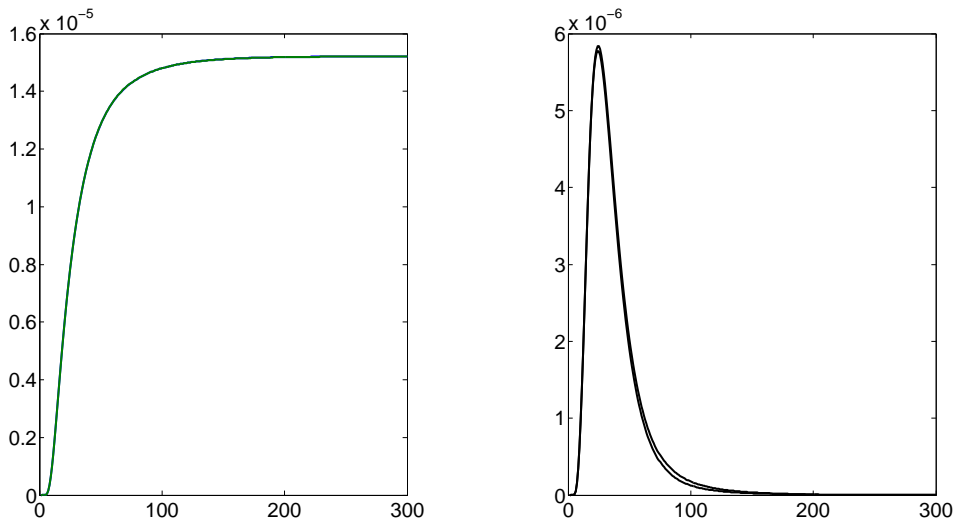


Figure 3.2: Two signals, modelled in the batch mode, coalesce, but can be vaguely distinguished if modelled in the injection mode.

necessarily applicable to the biosensor signals corresponding to arbitrary $x \in X$. It would be of interest to see whether the evaluations in [60, 75] failed for the data similar to that illustrated in Fig. 3.2 however the authors of these papers have not commented the cases of failures. A disadvantage of the artificial neural network-based method is in the implicit tackling of the difficulties mentioned above, since the optimization algorithm is hidden in the training procedure.

The analysis of biosensor signals, corresponding to the rough discretization of X , indicates that the problem considered is likely to be ill-defined. Another serious difficulty is caused by the time-consuming computations, needed to model a biosensor signal.

3.3 Statement of the relevant optimization problem

The minimization of $f(W, Z(x))$, where $Z(x)$ were modelled at every call of the subroutine of computation of an objective function value, would be very time-consuming as indicated above. Therefore the computation of $y(\cdot)$ is replaced by the computation of the interpolator $\tilde{y}(\cdot)$, where the value $\tilde{y}_j(t_i, x_j)$ is obtained by interpolating of values $y_j(t_i, k)$, $k = 1, 2, \dots, 64$ using a cubic spline. The values of $\tilde{y}(\cdot)$ are computed by a subroutine which uses the coefficients of splines evaluated in advance. For the latter evaluation, a set of 264 biosensor signals was modelled: $y_j(t_i, k)$, $j \in \{1, 2, 3, 4\}$, $t_i \in T$, $k = 1, 2, \dots, 64$. The approximation precision has been evaluated statistically: 1000 vectors x were generated randomly with a uniform distribution over X and a relative error of approximating $y(\cdot)$ by $\tilde{y}(\cdot)$ was computed similarly as (3.20). The mean value of the relative error (computed as by a formula similar to (3.20)) was equal to $6.1158 \cdot 10^{-7}$, and its standard deviation was equal to $5.3274 \cdot 10^{-6}$.

The quadratic measure of difference (3.18) seems to be suited for application of the gradient local descent methods. However, some experimentation has shown that for such an objective function the well recognized local descent algorithm from the MATLAB Optimization toolbox terminates not necessarily close to the solution. Since in these experiments the first-order necessary optimality conditions have been satisfied with a high precision, the objective function should be recognized as multimodal. The results of some experiments with local non-differentiable minimization algorithms for the objective function, defined as the measure of difference corresponding to the Chebyshev norm, were also not promising. Therefore, the global optimization method is needed for the problem considered [82].

The minimization problem (3.17-3.18), where the summands of $z(\cdot, x)$ are approximated by cubic polynomials, seems favorable to apply interval arithmetic-based

global optimization methods. However, the solution time for this type of problems is exceedingly high as shown in [81].

In this research, we do have no intention to select the global optimization algorithm most suitable for the minimization problem considered. Our goal is to investigate the suitability of the optimization-based approach to evaluate the concentrations of components of a mixture, and to establish the properties of the optimization problem that could be important in a further real-world implementation in the form of an embedded system. The experimental investigation of properties of the objective function has shown that its hypersurface can be characterized as a deep valley with a flat bottom, where first-order optimality conditions are fulfilled with rather a high precision. Therefore, a simple combination of the global random search with a local descent seems promising to find a point at the bottom of the valley with the objective function value, close to the global minimum.

A global search algorithm was developed taking into account the experimentally established features of $z(t, x)$. The first summand $y_1(t, \kappa)$ is linear with respect to the concentration variable κ during the entire transition process; see the left side of Fig. 3.3 where 64 graphs of $y_1(t, \kappa)/\kappa$, $\kappa = 1, \dots, 64$ are presented which, however, are all coincident. The fourth summand $y_4(t, \kappa)$ is highly nonlinear with respect to κ , and the range of $y_4(t, \kappa)$ is a small fraction of the range of $y_1(t, \kappa)$; see the right side of Fig. 3.3. The linearity of $y_1(t, \kappa)$ can be exploited to simplify the minimization of (3.18):

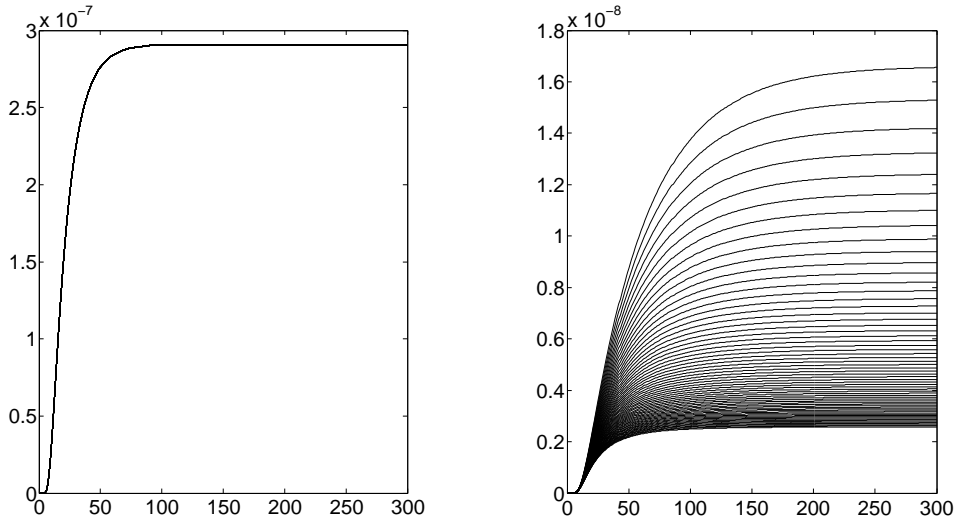


Figure 3.3: Graphs of normalized biosensor signals $y_j(t, \kappa)/\kappa$ ($j = 1$ on the left side, and $j = 4$ on the right side) drawn for $\kappa = 1, \dots, 64$, $t = 0, \dots, 300$. These graphs show that $y_1(t, \kappa)$ is linear with respect to the concentration κ during the whole transition time interval, while the signal $y_4(t, \kappa)$ is nonlinear

$$\begin{aligned}
 & \arg \min_{x_1} f_2(W, \tilde{Z}(x)) = \\
 & \arg \min_{x_1} \sum_{i=1}^{300} \left(w_i - x_1 \tilde{y}_1(t_i, 1) - \sum_{j=2}^4 \tilde{y}_j(t_i, x_j) \right)^2 = \\
 & \frac{\sum_{i=1}^{300} \left(w_i - \sum_{j=2}^4 \tilde{y}_j(t_i, x_j) \right) \cdot \tilde{y}_1(t_i, 1)}{\sum_{i=1}^{300} \tilde{y}_1^2(t_i, 1)}. \tag{3.21}
 \end{aligned}$$

Replacing x_1 by its optimal value x_{1opt} , we reduce the four-dimensional optimization problem to a three-dimensional one. The global search was performed by generating N_g random vectors (x_2, x_3, x_4) with a uniform distribution over the three-dimensional feasible region, and selecting g best points $(x_{1opt}, x_2, x_3, x_4)$. The latter were used as the starting points for the local descent. As seen in Fig. 3.3, the influence of $y_4(t, \kappa)$ on the objective function values can be relat-

ively weak, therefore termination conditions of the local descent should be set sufficient to guarantee the computation of the local minimizer with a high accuracy.

3.4 Numerical experiments

To investigate the precision of evaluation of concentrations, the biosensor signals were modelled under the conditions discussed above. The mixture contained four substrates characterized by $V_j = 10^{-6-j}$, $j \in \{1, 2, 3, 4\}$. The concentration of each substrate could vary in the interval $1 \leq x_j \leq 64$, and for each experiment below 1000 random vectors x with a uniform distribution over that region were generated to model the biosensor signals.

The first experiment was done to investigate the precision of the concentration evaluation in the batch mode. The global search was performed with the following parameters of the algorithm: $N_g = 1000$, $g = 5$. For the local minimization, the MATLAB subroutine *fmincon* was used with a user supplied gradient. The termination condition was defined by tolerances $TolFun = 10^{-4}$ for the values of objective function (3.18), multiplied by 10^7 (to accommodate the scale of the function values and the scale of the parameters of the algorithm), and by $TolX = 0.005$. The results are presented in Table 3.1, where Δx_j denotes the difference between the actual x_j and its evaluated value, and f_{\min} denotes a relative approximation error computed as in (3.20). The precision of the concentration evaluation of the first two substrates is quite good, while the evaluation of the accuracy of the last two substrates is insufficient. The low accuracy, obtained for the latter two substrates, can be explained by their insignificant input in to the biosensor signal. For the discussion about the significance of inputs of the considered substrates to the signal of a biosensor we refer to Section 3. This diversity in precision is also well illustrated by the following example: a relative discrepancy

Table 3.1: Precision of the evaluation of concentrations in the batch mode for the biosensor with the layer $d = 0.02\text{cm}$ wide

| | f_{\min} | Δx_1 | Δx_2 | Δx_3 | Δx_4 |
|------|------------------------|--------------|--------------|--------------|--------------|
| mean | $2.5520 \cdot 10^{-4}$ | 0.6304 | 0.5139 | 9.3593 | 19.4844 |
| std | $4.0538 \cdot 10^{-4}$ | 0.9354 | 0.6951 | 15.1093 | 15.3593 |

Table 3.2: Precision of the evaluation of concentrations in the injection mode for the biosensor with the layer $d = 0.02\text{cm}$ wide

| | f_{\min} | Δx_1 | Δx_2 | Δx_3 | Δx_4 |
|------|------------------------|--------------|--------------|--------------|--------------|
| mean | $2.8495 \cdot 10^{-5}$ | 0.0041 | 0.0108 | 0.0408 | 0.0464 |
| std | $3.1573 \cdot 10^{-4}$ | 0.0388 | 0.1663 | 0.8404 | 0.9755 |

between two signals, corresponding to $x = (44.5764, 62.3342, 16.0006, 38.7044)$ and to $x = 43.0724, 63.1362, 35.9738, 15.8452$, computed according to (3.20) is negligible since it is equal to $3.7361 \cdot 10^{-4}$.

The second experiment was performed with the same conditions as above, but in the injection measurement mode. The results, presented in Table 3.2 show that the accuracy of this evaluation method is quite acceptable in practice. A similar conclusion can be drawn from the results of the experiments, presented in Table 3.3, where the constructive parameter of the biosensor d is varied around the basic value.

The optimization-based evaluation of concentrations under general conditions of

Table 3.3: Precision of evaluation of concentrations in the injection mode for the biosensors with the layer $d = 0.01\text{cm}$ width and $d = 0.03\text{cm}$ wide

| $d = 0.01$ | | | | | |
|------------|------------------------|--------------|--------------|--------------|--------------|
| | f_{\min} | Δx_1 | Δx_2 | Δx_3 | Δx_4 |
| mean | $6.2751 \cdot 10^{-5}$ | 0.0024 | 0.0553 | 0.4929 | 0.4498 |
| std | $2.2811 \cdot 10^{-4}$ | 0.0123 | 0.2489 | 2.0472 | 1.8462 |
| $d = 0.03$ | | | | | |
| | f_{\min} | Δx_1 | Δx_2 | Δx_3 | Δx_4 |
| mean | $1.8358 \cdot 10^{-4}$ | 0.0945 | 0.1133 | 0.1106 | 0.3823 |
| std | $6.2409 \cdot 10^{-4}$ | 0.3029 | 0.3506 | 0.3945 | 1.2043 |

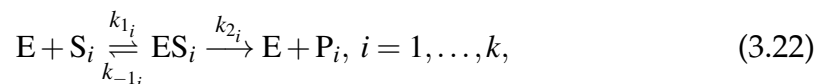
the modelled experiment yields the results of acceptable to the praxis precision. Note that a very simple optimization algorithm has been used. The optimization precision could be enhanced, but it does not seem reasonable because of an inevitably restricted precision of the modelling algorithm. From the point of view of real-world applications, a further investigation of the problem is urgent, taking into account the interaction between separate enzyme reactions, and measurement errors. Optimization in the presence of noise is considerably more difficult than that without noise. On the other hand, in practical problems optimization can possibly be facilitated by narrower intervals of the model parameters (which define the measurement conditions) than that in the present paper. Selection of the most suitable optimization algorithm is of especial interest taking into account the requirements of the potential implementation in an embedded measurement system.

3.5 Further development of the biosensor model

The discussed model, however is developed further since the interaction between substances was not evaluated in the first research part. This section involves evaluation of interaction between substrates. The model as well as software tool were developed to support this model and output of the results for further analysis.

3.5.1 Mathematical model

We consider a mono-enzyme multi-biosensor (many substrates) using the Michaelis-Menten kinetics [33, 71, 83],



where E denotes the enzyme, S_i is the substrate, ES_i stands for the complex of enzyme and substrate, P_i is the reaction product, kinetic constants k_{1_i} , k_{-1_i} and k_{2_i} correspond to the respective reactions: the enzyme substrate interaction, the reverse enzyme substrate decomposition and the product formation, and k is the number of substrates to be analyzed.

When substrates S_1, \dots, S_k ($k > 1$) react with a single enzyme E without forming any multi-fold complex that contains two or more substrates, and the substrates do not combine directly with each other, then in mixtures of S_1, \dots, S_k each substrate acts as a competitive inhibitor of the others [32, 84].

The biosensor to be modelled is intended to analyze a mixture of k substrates (compounds). Practical mono-enzyme analytical systems are usually limited to determining only a few (often to two) substrates [83].

The reactions in the network (1.1) are usually of different rates [32, 33]. A large difference of timescales in the reactions creates difficulties for simulating the temporal evolution of the network and for understanding the basic principles of the biosensor operation. To sidestep these problems, the quasi-steady-state approach (QSSA) is often applied [34, 85, 86]. According to QSSA, the concentration of the intermediate complex does not change on the time-scale of product formation.

The amperometric biosensor is treated as an electrode and a relatively thin layer of an enzyme (enzyme membrane) applied onto the probe surface. The biosensor model involves two regions: the enzyme layer, where biochemical reactions (1.1) as well as the mass transport by diffusion take place, and a convective region where the concentrations of the substrates are maintained constant. Assuming a symmetrical geometry of the electrode and a homogeneous distribution of the immobilized enzyme in the enzyme layer of a uniform thickness, the mathematical model of the biosensor action can be defined in a one-dimensional-in-space

domain [15, 35].

3.5.2 Governing equations

Application of QSSA and coupling the enzyme-catalyzed reactions (1.1) in the enzyme layer with the one-dimensional-in-space diffusion, described by Fick's law, lead to the following system of equations of the reaction-diffusion type ($t > 0$):

$$\begin{aligned}\frac{\partial S_i}{\partial t} &= D_{S_i} \frac{\partial^2 S_i}{\partial x^2} - \frac{V_{max_i} S_i}{K_{M_i} \left(1 + \sum_{j=1}^k S_j / K_{M_j}\right)}, \\ \frac{\partial P_i}{\partial t} &= D_{P_i} \frac{\partial^2 P_i}{\partial x^2} + \frac{V_{max_i} S_i}{K_{M_i} \left(1 + \sum_{j=1}^k S_j / K_{M_j}\right)}, \quad i = 1, \dots, k, \quad 0 < x < d,\end{aligned}\tag{3.23}$$

where x and t stand for space and time, respectively, $S_i(x, t)$ and $P_i(x, t)$ correspond to the molar concentrations of the substrate S_i and the product P_i , respectively, V_{max_i} is the maximal enzymatic rate attainable with that amount of the enzyme when the enzyme is fully saturated with the substrate S_i , K_{M_i} is the Michaelis constant, d is the thickness of enzyme layer, D_{S_i} and D_{P_i} are the diffusion coefficients, $V_{max_i} = k_{2_i} E_0$, $K_{M_i} = (k_{-1_i} + k_{2_i}) / k_{1_i}$, and E_0 is the total concentration of the enzyme, $i = 1, \dots, k$.

3.5.3 Initial and boundary conditions

Let $x = 0$ represent an electrode surface, and $x = d$ correspond to the boundary between the enzyme layer and the bulk solution. The biosensor operation starts when all the substrates (S_1, \dots, S_k) appear in the bulk solution ($t = 0$),

$$\begin{aligned}S_i(x, 0) &= 0, \quad P_i(x, 0) = 0, \quad 0 \leq x < d, \\ S_i(d, 0) &= S_{0_i}, \quad P_i(d, 0) = 0, \quad i = 1, \dots, k,\end{aligned}\tag{3.24}$$

where S_{0i} is the concentration of the substrate S_i in the bulk solution, $i = 1, \dots, k$.

Due to the electrode polarization the concentrations of the reaction products (P_1, \dots, P_k) on the electrode surface ($x = 0$) are permanently reduced to zero ($t > 0$) [15],

$$P_i(0, t) = 0, \quad i = 1, \dots, k. \quad (3.25)$$

Since the substrates are not ionized, fluxes of their concentrations on the electrode surface were assumed to be zero ($t > 0$),

$$D_{S_i} \frac{\partial S_i}{\partial x} \Big|_{x=0} = 0, \quad i = 1, \dots, k. \quad (3.26)$$

The concentrations of the substrates and the products in the bulk solution remain constant during the biosensor operation,

$$S_i(d, t) = S_{0i}, \quad P_i(d, t) = 0, \quad i = 1, \dots, k. \quad (3.27)$$

3.5.4 Biosensor response

The biosensor current density $I(t)$ at time t was expressed explicitly from the Faraday and the Fick laws [32],

$$I_i(t) = n_i F D_{P_i} \frac{\partial P_i}{\partial x} \Big|_{x=0}, \quad i = 1, \dots, k, \quad (3.28a)$$

$$I(t) = \sum_{i=1}^k I_i(t), \quad (3.28b)$$

where $I_i(t)$ is the density of the Faradaic current, generated by the electrochemical reaction that involves oxidation or reduction of the product P_i , n_i is the number of electrons involved in a charge transfer at the electrode surface in the corresponding reaction, F is the Faraday constant.

We assume that the system approaches a steady-state as $t \rightarrow \infty$,

$$I_{\infty} = \lim_{t \rightarrow \infty} I(t), \quad (3.29)$$

where I_{∞} is the density of the steady-state biosensor current.

3.6 Section summary

In the mathematical modelling setting the optimization-based approach is efficient in evaluating concentrations of several substrates in a liquid, where the available data are modelled as an amperometric signal of a biosensor. An urgent problem of further research is extension of the obtained results to the case where the interaction between separate enzyme reactions is taken into account as well as complications caused by collecting data of real-world experiments.

The proposed optimization-based method of the quantitative analysis of biosensor response is appropriate for the evaluation of the concentrations of the substrates by single enzyme amperometric biosensors using the Michaelis-Menten kinetics 1.1.

A computer simulation, based on the mathematical model (3.23)–(3.27), can be used to generate pseudo-experimental biosensor responses to mixtures of substrates. The generated data can be used to validate a method of the quantitative analysis as well as to calibrate the analytical system.

Conclusions

Different amperometric biosensors were modelled by non-stationary reaction-diffusion equations, containing nonlinear terms, related to the kinetics of enzymatic reactions. Mathematical models were approximated by using finite difference computational schemes. A number of computer experiments were carried out, which leads us to the following conclusions:

- The dimensionless mathematical model, for selected biosensors, is appropriate to be used as a framework for numerical investigation of the impact of model parameters on the biosensor action and to optimize the biosensor configuration.
- The computational model of an amperometric mediated biosensor, based on an enzyme layer and two supporting porous membranes, are appropriate to investigate the kinetic peculiarities of the biosensor. The comparison of experimental and simulated results have showed that the model most accurately describes the biosensor operation at low concentrations of the substrate.
- By increasing the thickness of the external diffusion layer or by decreasing the substrate diffusivity in this layer (by decreasing the Biot number Bi), the calibration curve of the biosensor can be prolonged by a few orders of magnitude. At relatively large values of the Biot number, the half maximal effective concentration C_{50} is almost insensitive to changes in Bi

- The half-maximal effective concentration C_{50} exponentially increases with a decrease in the injection time T_F . The calibration curve of the biosensor, acting in the injection mode, can be prolonged by a few orders of magnitude only by decreasing the injection time T_F .
- In the mathematical modelling setting, the optimization-based approach is efficient to evaluate concentrations of several substrates in a liquid where the available data is modelled as an amperometric signal of a biosensor.

List of references

- [1] C. Fan, K. W. Plaxco, and A. J. Heeger, "Biosensors based on binding-modulated donor-acceptor distances," *Trends Biotechnology*, vol. 23, no. 4, pp. 186–192, 2005.
- [2] C. Dhand, M. Das, M. Datta, and B. Malhotra, "Recent advances in polyaniline based biosensors," *Biosensors and Bioelectronics*, vol. 20, p. 2811–2821, 2011.
- [3] P. T. Kissinger, "Biosensors — a perspective," *Biosensors and Bioelectronics*, vol. 20, p. 2512–2516, 2005.
- [4] Global Industry Analysts Inc., *Biosensors in medical diagnosis - a global strategic business report*, 2012.
- [5] E. C. Alocilja and S. M. Radke, "Market analysis of biosensors for food safety," *Biosensors and Bioelectronics*, vol. 18, p. 841–846, 2003.
- [6] C. R. Taitt, G. P. Anderson, and F. S. Ligler, "Evanescent wave fluorescence biosensors," *Biosensors and Bioelectronics*, vol. 20, no. 12, p. 2470–2487, 2005.
- [7] W. H. van der Schalia, R. R. James, and T. P. G. II, "Selection of a battery of rapid toxicity sensors for drinking water evaluation," *Biosensors and Bioelectronics*, vol. 22, no. 1, pp. 18–27, 2005.
- [8] B. D. Malhotra and A. Chaubey, "Biosensors for clinical diagnostics industry," *Sensors and Actuators B: Chemical*, vol. 91, p. 117–127, 2003.
- [9] L. Campanella, A. Nuccilli, M. Tomassetti, and S. Vecchio, "Biosensor analysis for the kinetic study of polyphenols deterioration during the forced thermal oxidation of extra-virgin olive oil," *Talanta*, vol. 74, p. 1287–1298,

- 2008.
- [10] P. V. Climent, M. L. M. Serralheiro, and M. J. F. Rebelo, "Development of a new amperometric biosensor based on polyphenoloxidase and polyethersulphone membrane," *Pure and Applied Chemistry*, vol. 73, no. 12, pp. 1993–1999, 2001.
- [11] A. Heller and B. J. Feldman, "Electrochemical glucose sensors and their applications in diabetes management," *Chemical Reviews*, vol. 108, p. 2482–2505, 2008.
- [12] S. Song, H. Xu, and C. Fan, "Potential diagnostic applications of biosensors: current and future directions," *International Journal of Nanomedicine*, vol. 1, no. 4, pp. 433–440, 2006.
- [13] A. Sassolas, L. J. Blum, and B. D. Leca-Bouvier, "Immobilization strategies to develop enzymatic biosensors," *Biotechnology Advances*, vol. 30, p. 489–511, 2012.
- [14] I. Palchetti and M. Mascini, *Biosensor Technology: A Brief History*, vol. 54. Springer Netherlands, 2010.
- [15] T. Schulmeister, "Mathematical modeling of the dynamic behaviour of amperometric enzyme electrodes," *Selective electrode reviews*, vol. 12, pp. 203–260, 1990.
- [16] J. Kernevez, *Enzyme Mathematics. Studies in Mathematics and its Applications*. Amsterdam: Elsevier Science, 1980.
- [17] W. Press, S. Teukolsky, W. Vetterling, and B. Flannery, *Numerical Recipes in C: The Art of Scientific Computing*. Cambridge: Cambridge University Press, 2 ed., 1992.
- [18] W. Press, S. Teukolsky, W. Vetterling, and B. Flannery, *Numerical Recipes: The Art of Scientific Computing*. New York: Cambridge University Press, 3 ed., 2007.
- [19] A. Turner, I. Karube, and G. Wilson, *Biosensors: Fundamentals and Applications*. Oxford: Oxford University Press, 1987.

- [20] R. Monošik, M. Stred'ansky, and E. Šturdik, "Biosensors — classification, characterization and new trends," *Acta Chimica Slovaca*, vol. 5, pp. 109–120, 2012.
- [21] A. McNaught and A. Wilkinson, *IUPAC. Compendium of Chemical Terminology, 2nd ed.* Blackwell Scientific Publications, Oxford, 1997.
- [22] D. Thevenot, K. Toth, R. Durst, and G. Wilson, "Electrochemical biosensors: Recommended definitions and classification," *Pure and Applied Chemistry*, vol. 71, pp. 2333–2348, 1999.
- [23] A. Ghindilis, P. Atanasov, M. Wilkins, and E. Wilkins, "Immunosensors: electrochemical sensing and other engineering approaches," *Biosensors and Bioelectronics*, vol. 13, pp. 113–131, 1998.
- [24] A. J. Bäumner and R. Schmid, "Development of a new immunosensor for pesticide detection: a disposable system with liposome-enhancement and amperometric detection," *Biosensors and Bioelectronics*, vol. 13, pp. 519–529, 1998.
- [25] M. F. Yulaev, R. A. Sitdikov, N. M. Dmitrieva, E. V. Yazynina, A. V. Zherdev, and B. B. Dzantiev, "Development of a potentiometric immunosensor for herbicide simazine and its application for food testing," *Sensors and Actuators B*, vol. 75, pp. 129–135, 2001.
- [26] M. S. Wilson and R. D. Rauh, "Novel amperometric immunosensors based on iridium oxide matrices," *Biosensors and Bioelectronics*, vol. 19, pp. 693–699, 2004.
- [27] F. Darain, S. P. Doeg, J. S. Park, S. C. Chang, and Y. B. Shim, "A separation-free amperometric immunosensor for vitellogenin based on screen-printed carbon arrays modified with a conductive polymer," *Biosensors and Bioelectronics*, vol. 20, pp. 1780–1787, 2007.
- [28] K. Rogers, "Biosensors for environmental applications," *Biosensors and Bioelectronics*, vol. 10, pp. 533–541, 1995.
- [29] S. Krishnamoorthy, V. Makhijani, M. Lei, M. Giridharan, and T. Tisone,

- “Computational studies of membrane-based test formats,” in *2000 international conference on modeling and simulation of microsystems, technical proceedings*, pp. 590–593, 2000.
- [30] S.-J. Park, T. A. Taton, and C. A. Mirkin, “Array-based electrical detection of dna with nanoparticle probes,” *Science*, vol. 295, pp. 1503–1506, 2002.
- [31] J. Wang, “Electrochemical glucose biosensors,” *Chemical Reviews*, vol. 108, p. 814–825, 2008.
- [32] H. Gutfreund, *Kinetics for the Life Sciences*. Cambridge: Cambridge University Press, 1995.
- [33] F. W. Scheller and F. Schubert, *Biosensors*. Amsterdam: Elsevier Science, 1992.
- [34] L. Segel and M. Slemrod, “The quasi-steady-state assumption: a case study in perturbation,” *SIAM Review*, vol. 31, pp. 446–477, 1989.
- [35] R. Baronas, F. Ivanauskas, and J. Kulys, *Springer Series on Chemical Sensors and Biosensors*, vol. 9. Dordrecht: Springer, 2010.
- [36] J. Kulys, “The development of new analytical systems based on biocatalysts,” *Analytical Letters*, vol. 14, pp. 377–397, 1981.
- [37] P. Bartlett and R. Whitaker, “Electrochemical immobilisation of enzymes. part i. theory,” *Journal of Electroanalytical Chemistry*, vol. 224, pp. 27–35, 1987.
- [38] J. Aaron, M. Valenzuela, M. Pena, F. Salinas, and M. Mahedero, “Quantitative analysis of sulfadiazine using photochemically induced fluorescence detection in bulk solution and in a flow injection system,” *Analytica Chimica Acta*, vol. 314, p. 45–50, 1995.
- [39] P. Butler, W. Hamilton, L. Magid, T. Slawicki, Z. Han, and J. Hayter, “Effect of a solid/liquid interface on bulk solution structures under flow,” *Physica B: Condensed Matter*, vol. 241–243, p. 1074–1076, 1997.
- [40] R. Baronas, F. Ivanauskas, and J. Kulys, “Modelling dynamics of amperometric biosensors in batch and flow injection analysis,” *Journal of Mathematical Chemistry*, vol. 32, pp. 225–237, 2002.

- [41] D. Britz, *Digital Simulation in Electrochemistry, Lecture Notes in Physics*, vol. 666. Berlin: Springer, 2005.
- [42] D. Britz, R. Baronas, E. Gaidamauskaitė, and F. Ivanauskas, "Further comparisons of finite difference schemes for computational modelling of biosensors," *Nonlinear Analysis: Modelling and Control*, vol. 14, pp. 419–433, 2009.
- [43] H.-L. Schmidt, "Biosensors and flow injection analysis in bioprocess control," *Journal of Biotechnology*, vol. 31, pp. v–vi, 1993.
- [44] L. Mello and L. Kubota, "Review of the use of biosensors as analytical tools in the food and drink industries," *Food Chemistry*, vol. 77, pp. 237–256, 2002.
- [45] R. Nenkova, R. Atanasova, D. Ivanova, and T. Godjevargova, "Optimal inputs and sensitivities for parameter estimation in bioreactors," *Biotechnology & Biotechnological Equipment*, vol. 24, p. 1986, 2010.
- [46] H. Lüdi, M. Garn, P. Bataillard, and H. Widmer, "Flow-injection analysis and biosensors - applications for biotechnology and environmental-control," *Journal of Biotechnology*, vol. 14, pp. 71–79, 1990.
- [47] M. Kim and M.-J. Kim, "Isocitrate analysis using a potentiometric biosensor with immobilized enzyme in a fia system," *Food Research International*, vol. 36, no. 3, p. 223–230, 2003.
- [48] F. Vianello, S. Ragusa, M. T. Cambria, and A. Rigo, "A high sensitivity amperometric biosensor using laccase as biorecognition element," *Biosensors and Bioelectronics*, vol. 21, no. 11, p. 2155–2160, 2006.
- [49] F. Tasca, L. Gorton, J. B. Wagnerb, and G. Nöll, "Increasing amperometric biosensor sensitivity by length fractionated single-walled carbon nanotubes," *Biosensors and Bioelectronics*, vol. 24, p. 272–278, 2008.
- [50] C. Tran-Minh, "Biosensors in flow-injection systems for biomedical analysis, process and environmental monitoring," *Journal of Molecular Recognition*, vol. 9, pp. 658–663, 1996.
- [51] B. Prieto-Simon, M. Campas, S. Andreescu, and J. Marty, "Trends in flow-

- based biosensing systems for pesticide assessment," *Sensors*, vol. 6, pp. 1161–1186, 2006.
- [52] P. Cervini and E. Cavalheiro, "Recent biosensing developments in environmental security," *Journal of the Brazilian Chemical Society*, vol. 19, p. 836, 2008.
- [53] M. Piano, S. Serban, R. Pittson, G. Drago, and J. Hart, "Amperometric lactate biosensor for flow injection analysis based on a screen-printed carbon electrode containing meldola's blue-reinecke salt, coated with lactate dehydrogenase and nad(+)," *Talanta*, vol. 82, pp. 34–37, 2010.
- [54] M. Oliveira, M. Lanza, A. Tanaka, and M. Sotomayor, "Flow injection analysis of paracetamol using a biomimetic sensor as a sensitive and selective amperometric detector," *Analytical Methods*, vol. 2, pp. 507–512, 2010.
- [55] S. Zhan, H. Zhao, and R. John, "A theoretical model for immobilized enzyme inhibition biosensors," *Electroanalysis*, vol. 13, pp. 1528–1534, 2001.
- [56] R. Baronas, J. Kulys, K. Petrauskas, and J. Razumienė, "Modelling carbon nanotube based biosensor," *Journal of Mathematical Chemistry*, vol. 49, pp. 995–1010, 2011.
- [57] M. Lyons, "Modelling the transport and kinetics of electroenzymes at the electrode/solution interface," *Sensors*, vol. 6, pp. 1765–1790, 2006.
- [58] F. Ivanauskas and R. Baronas, "Modelling an amperometric biosensor acting in a flowing liquid," *International Journal for Numerical Methods in Fluids*, vol. 56, pp. 1313–1319, 2008.
- [59] F. Ivanauskas, I. Kaunietis, V. Laurinavičius, J. Razumienė, and R. Šimkus, "Apparent michaelis constant of the enzyme modified porous electrode," *Journal of Mathematical Chemistry*, vol. 43, pp. 1516–1526, 2008.
- [60] R. Baronas, F. Ivanauskas, R. Maslovskis, M. Radavičius, and P. Vaitkus, "Locally weighted neural networks for an analysis of the biosensor response," *Kybernetika*, vol. 43, no. 1, pp. 21–30, 2007.
- [61] C. Amatore, A. Oleinick, I. Svir, N. da Mota, and L. Thouin, "Theoretical

- modeling and optimization of the detection performance: a new concept for electrochemical detection of proteins in microfluidic channels," *Nonlinear Analysis: Modelling and Control*, vol. 11, pp. 345–365, 2006.
- [62] M. Lyons, "Transport and kinetics at carbon nanotube - redox enzyme composite modified electrode biosensors," *International Journal of Electrochemical Science*, vol. 4(1), pp. 77–103, 2009.
- [63] D. Olea, O. Viratelle, and C. Faure, "Polypyrrole-glucose oxidase biosensor - effect of enzyme encapsulation in multilamellar vesicles on analytical properties," *Biosensors and Bioelectronics*, vol. 23, pp. 788–794, 2008.
- [64] O. Štikonienė, F. Ivanauskas, and V. Laurinavičius, "The influence of external factors on the operational stability of the biosensor response," *Talanta*, vol. 81, pp. 1245–1249, 2010.
- [65] L. Michaelis and M. M. L. Menten, "The kinetics of invertase action (translated by roger s. goody and kenneth a. johnson)," *FEBS Letters*, vol. 587, pp. 2712–2720, 2013.
- [66] E. Assibas, H. Bisswanger, A. Sotos-Lomas, M. Garcia-Moreno, F. Garcia-Canovas, J. Donoso-Pardo, F. Munoz-Izquierdo, and R. Varon, "A method, based on statistical moments, to evaluate the kinetic parameters involved in unstable enzyme systems," *Journal of Mathematical Chemistry*, vol. 44, pp. 379–404, 2008.
- [67] M. Lyons, T. Bannon, G. Hinds, and S. Rebouillat, "Reaction/diffusion at conducting polymer ultramicroelectrodes," *Analyst*, vol. 123, pp. 1961–1966, 1998.
- [68] S. A. Giner, R. M. T. Irigoyen, S. Cicuttin, and C. Fiorentini, "The variable nature of biot numbers in food drying," *Journal of Food Engineering*, vol. 101, no. 2, p. 214–222, 2010.
- [69] D. Gough and J. Leyboldt, "Membrane-covered, rotated disk electrode," *Analytical Chemistry*, vol. 51, pp. 439–444, 1979.
- [70] D. Šimelevičius, R. Baronas, and J. Kulys, "Modelling of amperometric

- biosensor used for synergistic substrates determination," *Sensors*, vol. 12, pp. 4897–4917, 2012.
- [71] A. Turner, I. Karube, and G.S.Wilson, *Biosensors: Fundamentals and Applications*. Oxford University Press, 1990.
- [72] J. Ruzicka and E. Hansen, *Flow Injection Analysis*. Wiley, New York, 1988.
- [73] S. van Stroey-Beelen, F. M. Everaerts, L. J. J. Janssen, and R. A. Tacken, "Diffusion-coefficients of oxygen, hydrogen-peroxide and glucose in a hydrogel," *Analytica Chimica Acta*, vol. 273, pp. 553–560, 1993.
- [74] J. Razumienė, J. Gurevičienė, J. Barkauskas, V. Bukauskas, and A. Šetkus, "Novel combined template for amperometric biosensors with changeable selectivity," in *Proceedings of the International Conference on Biomedical Electronics and Devices*, Biodevices, (Porto), pp. 448–452, 2009.
- [75] R. Baronas, F. Ivanauskas, R. Maslovskis, and P. Vaitkus, "An analysis of mixtures using amperometric biosensors and artificial neural networks," *Journal of Mathematical Chemistry*, vol. 36(3), pp. 281–297, 2004.
- [76] G. Seber and C. Wild, *Nonlinear Regression*. Wiley, Hoboken, 2003.
- [77] G. Dzemyda, V.Šaltenis, and V.Tiešis, *Optimizavimo Metodai*. Matematikos ir informatikos institutas, 2007.
- [78] Törn and Žilinskas, "Global optimization. lecture notes in computer science," *Analytical Chemistry*, vol. 350, pp. 1–255, 1989.
- [79] Křivý, Tvrdík, and Krepec, "Stochastic algorithms in nonlinear regression," *Computational Statistics and Data Analysis*, vol. 33, pp. 277–290, 2000.
- [80] A. Žilinskas, "Small sample estimation of parameters for wiener process with noise," *Communications in Statistics—Theory and Methods*, vol. 40, pp. 3020 – 3028, 2011.
- [81] A. Žilinskas and J. Žilinskas, "Interval arithmetic based optimization in nonlinear regression," *Informatika*, vol. 21, no. 1, pp. 149–158, 2010.
- [82] G. Dzemyda and L. Sakalauskas, "Optimization and knowledge-based technologies," *Informatika*, vol. 20(3), pp. 165–172, 2009.

- [83] T. Pocklington and J. Jeffery, "Competition of two substrates for a single enzyme. a simple kinetic theorem exemplified by a hydroxy steroid dehydrogenase reaction," *Biochemical Journal*, vol. 112, no. 3, pp. 331–334, 1969.
- [84] J. Kulys and R. Baronas, "Modelling of amperometric biosensors in the case of substrate inhibition," *Sensors*, vol. 6, no. 11, pp. 1513–1522, 2006.
- [85] B. Li, Y. Shen, and B. Li, "Quasi-steady-state laws in enzyme kinetics," *The Journal of Physical Chemistry A*, vol. 112, no. 11, pp. 2311–2321, 2008.
- [86] B. Li and B. Li, "Quasi-steady-state laws in reversible model of enzyme kinetics," *Journal of Mathematical Chemistry*, vol. 51, no. 10, pp. 2668–2686, 2013.

Darius Baronas

COMPUTER AIDED MODELLING OF MULTILAYER BIOSENSORS AND
OPTIMIZATION BASED PROCESSING OF AMPEROMETRIC
MEASUREMENTS

Doctoral dissertation

Physical sciences (P 000)

Informatics (09 P)

Informatics, System Theory (P 175)

Darius Baronas

DAUGIASLUOKSNIŲ BIOJUTIKLIŲ KOMPIUTERINIS MODELIAVIMAS IR
OPTIMIZAVIMO METODAIS GRĮSTA MATAVIMŲ METODIKA

Daktaro disertacija

Fiziniai mokslai (P 000)

Informatika (09 P)

Informatika, Sistemų teorija (P 175)